Journal of Medicinal Chemistry

Article

Discovery of Novel Potent Reversible and Irreversible Myeloperoxidase Inhibitors using Virtual Screening Procedure

Jalal Soubhye, Ibaa Chikh Alard, Iyas Aldib, Martine Prévost, Michel Gelbcke, Annelise De Carvalho, Paul G. Furtmüller, Christian Obinger, Joerg Flemmig, Sara Tadrent, Franck Meyer, Alexandre Rousseau, Jean Neve, Véronique Mathieu, Karim Zouaoui Boudjeltia, Francois M U Dufrasne, and Pierre G Van Antwerpen

J. Med. Chem., **Just Accepted Manuscript** • DOI: 10.1021/acs.jmedchem.7b00285 • Publication Date (Web): 03 Jul 2017

ACS Publications

Journal of Medicinal Chemistry is published by the American Chemical Society. 1155 Sixteenth Street N.W., Washington, DC 20036

Discovery of Novel Potent Reversible and Irreversible Myeloperoxidase Inhibitors using Virtual Screening Procedure

Jalal Soubhye[(1)*], Ibaa Chikh Alard[(2)], Iyas Aldib[(1)], Martine Prévost[(3)], Michel Gelbcke[(1)], Annelise De Carvalho[(4)], Paul G. Furtmüller[(5)], Christian Obinger[(5)], Jörg Flemmig[(6)], Sara Tadrent[(1)], Franck Meyer[(7)], Alexandre Rousseau[(8)], Jean Nève[(1)], Véronique Mathieu[(4)] Karim Zouaoui Boudjeltia[(8)], François Dufrasne[(1)§*], Pierre Van Antwerpen[(1,9)§*]

(1) Laboratoire de Chimie Pharmaceutique Organique, Faculté de Pharmacie, Université Libre de Bruxelles, Campus de la Plaine, Boulevard du Triomphe, 1050 Bruxelles, Belgium.

(2) Laboratoire de Pharmacie Galénique et Biopharmacie, Faculté de Pharmacie, Université Libre de Bruxelles, Campus de la Plaine, Boulevard du Triomphe, 1050 Bruxelles, Belgium.

(3) Laboratoire de Structure et Fonction des Membranes Biologiques, Université Libre de Bruxelles, Campus de la Plaine, Boulevard du Triomphe, 1050 Bruxelles, Belgium.

(4) Laboratoire de Cancérologie et Toxicologie Expérimentale, Faculté de Pharmacie, Université Libre de Bruxelles, Campus de la Plaine, Boulevard du Triomphe, 1050 Bruxelles, Belgium.

(5) Department of Chemistry, BOKU−University of Natural Resources and Life Sciences, Vienna, Austria.

(6) Institute for Medical Physics and Biophysics, Medical Faculty, University of Leipzig, Haertelstrasse 16–18, 04107 Leipzig, Germany.

(7) Laboratory of Biopolymers and Supramolecular Nanomaterials, Faculty of Pharmacy, Université Libre de Bruxelles (ULB), Campus de la Plaine, Boulevard du Triomphe, 1050 Bruxelles, Belgium.

(8) Laboratory of Experimentral Medicine, CHU Charleroi, A. Vesale Hospital, and Université Libre de Bruxelles, 6110 Montigny-le-Tilleul, Belgium.

(9) Analytical Platform of the Faculty of Pharmacy, Université Libre de Bruxelles, Campus de la Plaine, Boulevard du Triomphe, 1050 Bruxelles, Belgium.

Abstract

The heme enzyme myeloperoxidase (MPO) participates in innate immune defense mechanism through formation of microbicidal reactive oxidants. However, evidence has emerged that MPO-derived oxidants contribute to propagation of inflammatory diseases. Because of the deleterious effects of circulating MPO, there is a great interest in the development of new efficient and specific inhibitors. Here, we have performed a novel virtual screening procedure, depending on ligand-based pharmacophore modeling followed by structure-based virtual screening. Starting from a set of 727,842 compounds, 28 molecules were selected by this virtual method and tested on MPO *in vitro*. Twelve out of 28 compounds were found to have an IC_{50} less than 5 μM. The best inhibitors were 2-(7-methoxy-4-methylquinazolin-2-yl)guanidine (**28**) and (R)-2-(1-((2,3-dihydro-1*H*-imidazol-2-yl)methyl)pyrrolidin-3-yl)-5-fluoro-1*H*-benzo[d]imidazole (**42**) with IC_{50} values of 44 and 50 nM, respectively. Studies on the mechanism of inhibition suggest that **28** is the first potent mechanism-based inhibitor and inhibits irreversibly MPO at nanomolar concentration.

1. Introduction

The heme enzyme myeloperoxidase (MPO, EC 1.11.2.2) is a lysosomal protein that plays an important role in the human innate immunity system. It is expressed in neutrophils and stored in their azurophilic granules[1-5]. After phagocytosis of pathogens by the neutrophils, MPO is able to catalyze the H_2O_2-mediated oxidation of chloride to the powerful oxidizing agent hypochlorous acid (HOCl), which leads to the oxidation (degradation) of biomolecules of pathogens in the phagosome. Other halide (Br^-, I^- but not F^-) or pseudo-halide (SCN^-) ions can also act as substrates for MPO. Native ferric MPO [Por-Fe(III)] is oxidized by H_2O_2 to Compound I [$^{\bullet+}$Por-Fe(IV)=O, i.e. oxoiron(IV) porphyryl radical]. Compound I directly oxidizes SCN^-, I^-, Br^- or Cl^- to the corresponding (pseudo)hypohalous acids (HOX) thereby

restoring the ferric state (**Figure 1**)[6,7]. Other electron donors such as tyrosine, serotonin or tryptamine are oxidized via a one-electron pathway resulting in the formation of Compound II [Por-Fe(IV)-OH, i.e. oxoiron(IV)]. Finally, reduction of Compound II (which is outside the halogenation cycle) restores MPO in the native state (**Figure 1**)[8]. Although the reaction of Compound I with SCN^-, I^- and Br^- is faster than with Cl^-, HOCl is considered as the essential reaction product of MPO because of the high Cl^- concentration in human blood plasma compared to the other species[9].

In some cases, MPO is released from neutrophils, producing HOCl in the circulation which results in oxidative damages of the host tissues. These damages sometimes contribute to the development of injuries, e.g. in the kidney, the central nervous system, lung or the cardiovascular system[3]. The close relation between MPO activity and cardiovascular diseases prompted a study on the roles of the MPO/H_2O_2/Cl^- system in atherosclerosis. It has been reported that MPO can oxidize low-density lipoproteins (LDLs) thereby promoting an inflammatory response in monocytes and endothelial cells[3]. This inflammation results in the formation of foam cells in the artery walls, thus generating a necrotic center of atherosclerosis. Some evidences highlighted the role of MPO in the oxidation of high-density lipoproteins (HDLs), causing a decrease in their capacity to remove cholesterol from atherosclerotic lesions[10]. It is well documented that the MPO/H_2O_2/Cl^- system also contributes to decrease the concentration of $NO^{\bullet}$, and activates the protease cascades and fibrin deposition. As a result, the dysfunction of endothelial cells causes vulnerable plaques [11].

The role of the MPO/H_2O_2/Cl^- system in the inflammatory syndromes makes MPO a promising target for the development of new anti-inflammatory agents[12]. Several MPO inhibitors were already identified. Most of these compounds were obtained by drug design and comprise 3-aminoalkyl fluoroindole derivatives[13], aromatic hydroxamates[14] and indazoles[15]. **Figure 2** illustrates the most potent MPO inhibitors discovered until now that can

inhibit MPO at the nanomolar range.

By now, the structures of human MPO unbound or in complex with fairly small anions (halides, thiocyanate, cyanide) or covalently-bound to 2-thioxanthine have been determined[16, 17]. The crystal structure of salicylhydroxamic acid (SHA) bound to human MPO has also been described though no structure has been deposited in the PDB[18]. Recently, the X-ray structure of human MPO complexed to 2-((3,5-bis(trifluoromethyl)benzyl)amino)-N-hydroxy-4-oxo-1,4-dihydropyrimidine-5-carboxamide **(**compound **1)** has been solved (**Figure 2**)[14]. These structural data were used in the docking experiments for three main purposes: 1) to predict the interaction between the inhibitors and the active site 2) to implement structure activity relationship (SAR) for designing potent MPO inhibitors[19] and 3) to find ligands selected by virtual screening from available databases[20, 21].

Up to now, two virtual screening experiments were done to determine new MPO inhibitor scaffolds. The first one performed by Malvezzi *et al.*[22] using GOLD docking program screened the full Zinc database. The second was carried out by Aldib *et al.*[20] using Glide® as a software and ASINEX® as the ligand database. In our paper, four pharmacophore models were designed based on the most potent MPO inhibitors using LigandScout®[23-25]. These pharmacophore models were used to screen a filtered Zinc database. Compounds selected from this virtual screening were docked into the heme cavity of MPO by means of the LeadIT® docking program[26] to screen the Zinc database for potential ligands[27]. The best compound was selected as a hit, followed by the synthesis and evaluation of several analogues.

2. Results

Pharmacophore design

In this study, we applied a four-step computer-aided protocol to select compounds to be tested *in vitro* (**Figure 3**). The whole process included successively a Lipinski's rule filter, a screening based on the derivation of a pharmacophore, a docking screening and a selection based on various drug-relevant properties (**Figure 3**).

First, the 727,842 compounds of the Zinc database molecules (http://zinc.docking.org) were screened following the Lipinski's rule filter to select drug-like molecules using DruLiTo software (ref : (http://www.niper.gov.in/pi_dev_tools/DruLiToWeb/DruLiTo_index.html). This filter selected 494,915 compounds. In the second step, pharmacophore models, featuring the 3D key chemical determinants required for binding to MPO, were generated using the structural data of the seven most potent MPO inhibitory compounds known so far (**Figure 2**). These molecules have been used alone or in combination. When each potent inhibitor was used individually to generate pharmacophore models, a small number of compounds from the 494,915 drug-like molecules previously filtered matched the pharmacophore features (less than 25 compounds in total from the seven pharmacophores). In contrast, when using three or more potent inhibitors to define a pharmacophore model, a large number of compounds resulted from the screening (more than 20,000 compounds in all cases). Finally using all possible pairs combining the seven most potent inhibitors, 21 pharmacophore models were obtained which featured a pharmacophore-fit score ranging from 50.9 to 68.4 %. About 11000 hit molecules were then retrieved from the pharmacophore screening against the 494,915 compounds of this filtered database.

Only the pharmacophore models that have a specificity ≥ 0.5 were kept, providing a number of compounds less than 500 for each model. Four models met this criterion (named model 1 to 4) as they contain, 273, 185, 106, and 6 molecules respectively (570 compounds in total) (**Figure 3**). They were obtained from the following pairs of active potent inhibitors: **6**[13] and **4**[28] for model 1, **1**[14] and **6**[13] for model 2, **4** and **2** for model 3[14] and **7**[29] and **1** for model 4

(**Figure 4**). Model 1 comprises one hydrogen bond acceptor (HBA), one hydrogen bond donor (HBD), one hydrophobic moiety (H), one positively charged group (PI), and 40 exclusion volumes (XVOLs). Model 2 contains one HBA, one aromatic group (AR), one HBD, and 33 XVOLs. Model 3 encompasses two H sites, one HBA, and 41 XVOLs. Finally, model 4 contains two HBA, two HBD, one AR, and 37 XVOLs (see **Figure 4, Figures S3, and Table S1**).

Docking calculations

In the next stage, compounds issued from the pharmacophore screening procedure were docked on the X-ray structure of human MPO complexed with thiocyanate (PDB 1DNU) using the FlexX software.

To validate the docking procedure, compound **1** which has well-established interactions with MPO was docked (**Figure 5**). The best-score docked pose of **1** featured the pyrimidine ring stacked on the pyrrole ring D of the heme, and the trifluoromethyl aromatic ring occupying the hydrophobic pocket at the entrance of the active site. The hydroxamic acid group lied in the center of the distal cavity, and both the carbonyl and hydroxyl oxygens formed hydrogen bonds with Gln91 and His95 residues. One of the pyrimidine nitrogens provided the main interaction with the heme propionate group, whereas the oxygen of the hydroxyl group was well positioned for a hydrogen bond with Asp94. The trifluoromethyl aromatic ring of the molecule extended toward the surface of the enzyme. These interactions formed in the docked pose of **1** are quite similar to those in the crystallographic structure[14] where its lowest root-mean square deviation computed on all heavy atoms (RMSD) was 0.39 Å, allowing for the validation of the docking procedure (**Figure 5A**). Compounds **6, 7** and 4 were also docked according to our procedure. The best pose of these ligands featured the same set of interactions as those predicted with Glide software[13, 28] **(Figure 5)**. The fluorophenyl moiety

of **4** occupied the hydrophobic pocket at the entrance of the active site. Noticeably, the fluorophenyl group of **1** defined as an AR in the pharmacophore models 2 and 4 was not the aromatic moiety, the pyrimidine, making the stacking with the pyrrole subunit of heme in the X-ray structure or the docking **(Figure 5)**. The indole and benzodioxole groups of **6** and **4**, respectively, were defined as H groups in the pharmacophore model 1 for **6** and in pharmacophore models 1 and 3 for **4**, where they formed a π-π interaction with the pyrrole ring in the docking experiments. In contrast, the indole groups of **6** and **7** were presented as AR groups in pharmacophore models 2 and 4, respectively, indeed make aromatic interactions in their docked poses.

From the docked compounds issued from the pharmacophore screening procedure, only ligands featuring a docking score < -8.0 kcal/mol were kept. These ligands represent the 10 % best scoring molecules from models 1, 2 and 3 (24, 20, 12 and 3 compounds, respectively) and the 50% best scoring molecules from model 4 (4 molecules). The inspection of the docked poses of these selected molecules showed that most of them make interactions with Glu102, Thr100 and/or Gln91.

Toxicological Evaluation and Drug-Like Profile

Finally, the OSIRIS® property explorer tool (www.organic-chemistry.org/prog/peo) was used to predict drug-likeness, toxicity risk, mutagenicity, irritant, and tumorigenic effects of the selected molecules. Only the compounds passing this filter were considered for future studies **(Figure 3)**. From this selection, 16, 8, 5 and 1 compounds from models 1 to 4 successfully passed through the last filtering step, respectively. Two of these compounds were repeated in two models to give a total of 28 molecules.

Validation of the screening procedure

To assess the specificity and the sensitivity of this protocol, a set of 20 molecules of various chemical structures containing 10 active and 10 inactive compounds on MPO was chosen from the literature (the results of the method validation are illustrated in **Table 1**). All the active compounds were selected by Lipinski's filter and OSIRIS explorer (except **14** which were derived from dihydro-naphtalene). As a result, the pharmacophore screening procedure selected all active compounds except thioxanthine derivative, with a total selectivity of 90% and nine out of ten active compounds have passed the docking filter. In addition, regarding the 10 inactive molecules, none passed all screening filters indicating that these filters can retain possible inactive compounds.

Finally, the selected molecules were filtered for Pan Assay Interference Compounds (PAINS) by the online filter (http://zinc15.docking.org/patterns/home/). Only **34** and **51** did not pass this filter (**Table S4**).

Inhibition of MPO Chlorination Activity

After the selection of compounds through virtual screening, their activities were assessed by the taurine chloramine assay[12] and their IC_{50} values were determined (**Table 2**). The *in vitro* tests revealed that 12 compounds have an IC_{50} smaller than 5 µM. Among them, 9, 2 and 1 compounds belonged to the pharmacophore models 1, 2 and 4, respectively (no molecule associated to model 3). The best activities were found for model 1.

Compounds **28**, **42** and **55** have attracted our attention owing to their low IC_{50} ranging from 44 to 130 nM. Remarkably, they displayed docking features similar to those of **5**, **6** and **4,** in particular an ionic interaction of their ammonium or guanidinium group with Glu102 (see **Figure 6**). Among the tested candidates, 5 drugs were found to have IC_{50} values less than 1 µM including **36**, **41**, **43** and **48** (**Table 2**). Other drugs were of particular interest such as the fluoroquinolones (**29** and **30**) due to good predicted interactions with the active site of the

enzyme, and the absence of inhibition. Pharmacophore modeling and docking experiments predicted that **38**, **40**, **44**, **47**, **49** and **51** had a high potency, but their inhibitory properties were low. These results suggest that other parameters such as the redox properties (of some of these compounds) play an important role in the inhibition of MPO, emphasizing the limitation of the virtual screening protocol[29].

In the light of these results, we decided to use Glide, another docking program[20], to dock the 12 active compounds in order to combine information about the binding modes predicted by both software. Overall the binding modes are rather comparable with, in most cases, the same aromatic moiety of each compound found to be stacked onto the pyrrole ring (**Table S2**). There are however a few exceptions such as compounds **34** and **43** with IC_{50} values of 1.15 and 0.35 μM, respectively, which feature a stacking of an aromatic moiety onto the heme in the docked pose produced by Glide though no stacking is observed with FlexX. In contrast the phtalazine structure of compound **36** (IC_{50} = 0.9 μM) is found to bind in a parallel mode on the heme pyrrole with FlexX only whereas Glide favors the interaction of the hydrazine group with Glu102.

Virtual evaluation of the active 12 compounds on mutated MPO (Glu102→Gln102)

In order to buttress the conjecture that this inhibitor indeed binds the MPO active site, the 12 most active compounds were docked in MPO with, Glu102, one residue shown by docking to interact with several inhibitors, substituted in silico into Gln (**Figures S5**). For most compounds carrying a positive charge, their binding modes predicted by Glide differ in the MPO variant compared to the wild-type and sustain the role of Glu102 in contributing to the binding of those compounds in the active site. In contrast, the binding mode of most compounds carrying no positive charge is not affected by Glu102 substitution.

Steady-state Activity Studies on the Mechanism of Inhibition

Myeloperoxidase inhibitors are classified in three main groups, namely (i) irreversible inhibitors (e.g. thioxanthine), (ii) compounds that promote accumulation of Compound II without binding to the active site (e.g. dapsone) and (iii) compounds that bind reversibly to the active site of MPO (e.g. SHA). Compounds from the second category may lose their inhibitory effects in a physiological environment because of the abundance of better peroxidase substrates such as ascorbate and tyrosine that restore ferric MPO by reduction of Compound II[14]. In order to decipher the mechanism of action of these inhibitors, ligands with $IC_{50} < 2.5$ μM (Compounds **28**, **34**, **35**, **36**, **41**, **42**, **43**, **48**, and **55**) were selected and their interaction with MPO was studied in the absence and presence of hydrogen peroxide. In practice, after 10 minutes of incubation, the enzyme was diluted 100-fold, and the residual chlorination activity was measured. Each inhibitor alone caused about 10-30 % inactivation of MPO, whereas hydrogen peroxide alone minimally affected activity. However, **28** or **36** in the presence of hydrogen peroxide caused an almost complete loss in enzyme activity. Chloride did not prevent enzyme inactivation by these compounds (**Table 3**). By contrast, combination of the other compounds with hydrogen peroxide did not cause more than 30 % inhibition. These data clearly suggest that MPO uses hydrogen peroxide to oxidize **28** and **36**, thereby irreversibly inactivating the enzyme[17].

Furthermore, we added 5 μM of **28** (a model of irreversible inhibitor) and **43** (a model of reversible inhibitor) to MPO in the presence of 30 μM of guaiacol. After incubation with or without hydrogen peroxide for 20 minutes, the reaction mixture was diluted 200 times and the residual peroxidase activity was assessed by following the increase of absorbance at 470 nm for 10 min[14]. **Figure 7** demonstrates that the activity of MPO in the presence of **28** cannot be recovered by dilution as long as H_2O_2 was present. In the absence of H_2O_2, there was no inhibition of MPO, clearly underlining that **28** is an irreversible mechanism-based inhibitor. By contrast, the effect of metoclopramide on the residual activity of MPO both in the

presence and absence of H_2O_2 was similar to that of DMSO, indicating that **43** acts as reversible MPO inhibitor (**Figure 7A**).

In order to see whether **43** can bind at the active site with a relatively low dissociation rate, another reversibility test was done. Tyrosine was used as a MPO substrate that converts MPO Compound I into Compound II and Compound II into native MPO, acting as a substrate for Compound I and II. DMSO was employed as a negative control while **43** in absence of tyrosine was used as a positive one. After adding 10 μM H_2O_2, the MPO activity was monitored by measuring the absorbance of 3,3′,5,5′-tetramethylbenzidine (TMB) during 10 minutes. As shown in **Figure 7B**, **43** can inhibit MPO even in the presence of tyrosine indicating that the inhibitor binds the active site, preventing tyrosine to enter the active pocket and oxidize Compound II to ferric enzyme.

Transient-State Kinetic Studies

Next, we probed the interaction of 5 compounds with the relevant redox intermediates of MPO, i.e. Compound I and Compound II (**Figure 1**)[9], by using multimixing stopped-flow spectroscopy. In detail, we aimed to study the mechanism of interaction involving irreversible inhibitors **28** and hydralazine, reversible inhibitor **43** and inactive compounds **40** and **29**. Compound I was pre-formed and probed for interaction with these molecules. Concerning **28** and hydralazine, an unusual behavior was observed (**Figure 8 and S2**). As with most inhibitors, Compound I was reduced via a one-electron reaction to Compound II, reflected by an increasing absorbance at 456 and 632 nm (**Figure 8A and C**). These reactions were fast with an apparent bimolecular rate constant k_3 of 1.98 X 10^6 M^{-1} s^{-1} and 1.7 X 10^6 M^{-1} s^{-1} for **28** and **36**, respectively (Table 4). Finally, the Compound II spectrum was converted (independently of the concentration of **28**) (**Figure 8D**) to a spectrum with a Soret maximum at 432 nm (accompanied by hypochromicity) and peaks at 570 and 626 nm. This spectrum

cannot be assigned to native MPO or Compound III (**Figure 8B**), but, interestingly, resembles that observed for MPO with covalently bound 2-thioxanthine[17].

With **40** and **43**, there was a direct and fast transition of Compound I to Compound II (Soret maximum at 456 nm) with clear isosbestic points (**Figure 9A**). The reactions were monophasic (inset to **Figure 9A**) and from the slope of the linear plot of k_{obs} values *versus* inhibitor concentration, the apparent bimolecular rate constant (k_3) of Compound I reduction was calculated (**Figure 9C**). Both molecules are good electron donors for Compound I (Table 3). As typical reversible inhibitors, **43** reduces Compound II back to ferric MPO (**Figure 9B and D**) at a slow rate (k_4 = 180 M^{-1} s^{-1}). The ratio of k_3/k_4 is high and as a consequence Compound II accumulates thereby reducing the chlorination activity of MPO.

The behavior of the two inactive molecules **40** and **29** was completely different. The successive transformations Compound I → Compound II →ferric MPO in the presence of **40** was very fast. The calculated apparent bimolecular rate constants of both reactions were k_3 = 5.2 × 10^6 M^{-1} s^{-1} and k_4 = 1.7 ×10^4 M^{-1} s^{-1}. Therefore, **40** does not mediate Compound II accumulation and thus (reversible) inhibition of the chlorination activity (Table 4). By contrast, **29** was shown to be a bad electron donor for Compound I (k_3 = 3.1 × 10^4 M^{-1} s^{-1}) and Compound II reduction to the ferric state could not be measured. However, there was a steady-state shift to Compound II similar to that seen with **28** and **36** (**Figure S8**). However, in contrast to the latter, **29** reacts very slowly with Compound I (**Table 4**) and thus cannot compete with chloride (140 mM) for Compound I reduction.

Determination of partition ratio for mechanism-based inhibitors

The transient-state kinetic studies on **28** and **36** together with the steady-state activity tests indicated that these ligands are mechanism-based irreversible inhibitors of MPO. The mechanism of irreversible interaction might include modification of the prosthetic group (e.g.

covalent bond formed between inhibitor and heme) or of the protein, whereas a reversible inhibitor (e.g. **43**) is released from the (unmodified) enzyme. Here, we probed the impact of different ratios of concentration of [inhibitor]/[MPO] on the remaining MPO activity. **Figure 10** demonstrates that the remaining MPO activity decreased as a linear function of [inhibitor]/[MPO] ratio and completely disappeared at [inhibitor]/[MPO] ratios of 67 and 110 for **28** and **36**, respectively. This suggests that on average one individual enzyme is able to cycle 67 times before being irreversibly inhibited by **28**. A completely different picture was obtained with the reversible inhibitor **43** (**Figure 10**) as no decrease of remaining MPO activity at increasing [**43**]/[MPO] ratios is observed.

Inhibition of LDL oxidation

Finally, we investigated the effect of these compounds on the MPO-mediated oxidation of LDL by using an enzyme-linked immunosorbent assay (ELISA) based on a mouse monoclonal antibody (Mab AG9) that specifically recognizes MPO-oxidized ApoB-100 on LDL. The obtained IC_{50} values are summarized in Table 3. Most of these molecules inhibit LDL oxidation at low μM concentrations. The hierarchy of IC_{50} values correlated with that of the taurine chlorination inhibition assay, but the absolute IC_{50} values obtained from the LDL oxidation assay were slightly increased. **28** exhibits the best LDL oxidation inhibitory activity with a calculated IC_{50} value of 90 nM. Interestingly, in this assay **43** did not show inhibitory activity.

Oxidation products of 36 and 28

The one-electron oxidation of **36** by horseradish peroxidase (HRP) is known to produce hydralazyl radicals which then decompose to form various products or react with molecular oxygen to generate reactive oxygen-centered radicals[38]. Here, we incubated MPO with **36** in phosphate-buffered saline (PBS), started the reaction by adding H_2O_2 and analyzed the

reaction mixture by LC-HRMS after 60 min of incubation. Phtalazine (MH^+ = 131.0606, error = -1.8 ppm) was the only detected reaction product (**Figure S10A**). Upon H_2O_2-mediated oxidation of **36** by HRP, this intermediate was also found as main reaction product.

In case of **28,** two reaction products were detected by LC-HRMS. Regarding the first derivative, the amino group of the guanidine was eliminated giving *N*′-(7-methoxy-4-methylquinazolin-2-yl)formimidamide (**28-OX-1**) (MH^+ = 217.0926, error = 0.42 ppm) (**Figure S10B**). The second detected compound was formed via the elimination of diamine-methylene group from the side guanidine group to give 2-amino-7-methoxy-4-methylquinazoline (**28-OX-2**) (MH^+ = 190.0973, error = 1.6 ppm) (**Figure S10C**). It is worthy to note that phtalazine and **28-OX-1** could not be detected when the experiment was performed without adding H_2O_2, while the metabolite **28-OX-2** was also found in the absence of H_2O_2, although in very low amounts.

Optimization of 28 Derivatives

Following the inhibition of taurine chlorination, compound **28** provides the best activity. This result prompted us to improve its activity. A series of *N*-(4-methyl-quinazolin-2-yl)-guanidines (**56-62**) was designed based on the features of the docking poses of **28**. The introduction of halogen atoms (F, Cl or Br) at positions 6 and 7 as well as displacement of methoxy group for hydrogen was probed by docking experiments (structures provided in table 5). It has resulted that candidate **56** (without HBA group) featured a shifted stacking pose, while compounds **58** and **59** (Br or Cl on position 6) had no stacking pose. Ligands **57** and **60** with fluorine on position 6 and 7 show the same interactions as **28** but with a lower affinity.

Subsequently, *N*-(4-Methyl-quinazolin-2-yl)-guanidine analogues were synthesized through Skraup reaction by incorporating the relevant aniline at a high dilution level, which led to the

corresponding 1,2-dihydro-2-methylquinoline. Treatment with cyanoguanidine gave the substituted *N*-(4-methyl-quinazolin-2-yl)-guanidines **56-62** (**Scheme 1**)[39].

These *N*-(4-methyl-quinazolin-2-yl)-guanidine derivatives were assayed by the taurine chloramine test to determine the respective IC_{50} values (**Table 5**). The most active molecules were **60** and **28** that possessed F and MeO substituents, respectively, at position 7. In addition, halogen atoms at the same position conferred a higher activity than compounds with a halogen atom at position 6. Finally, the absence of a functional group on the aromatic ring of **56** resulted in the lowest activity.

Compounds in Table 5 showed a variation of activity as a function of halogen atom following the order: F > Cl > Br. Docking experiments shed light on the *in vitro* results (**Figure 11**). All compounds from **60** to **62** functionalized with a halogen atom at position 7 featured stacking pose while those substituted with Br or Cl at position 6 featured a shifted stacking pose (**58** and **59)**. However, all *N*-(4-methyl-quinazolin-2-yl)-guanidine derivatives interacted with Glu102 and propionate of the active site through the guanidinium group. Regarding **60**, **61** and **62,** Thr100 appeared to be part of the anchoring site of MPO.

The effects of compounds 28 and 42 on human neutrophils

In comparison to the HOCl-producing activity observed in the absence of the inhibitor (the value was set to 100%) no clear inhibitory effect could be found when the concentration of compound **28** was up to 20 μM. In fact, while the addition of 1 or 5 μM of **28** led to a highly significant reduction of the relative chlorinating activity to about 67 – 71 %, the addition of 10 – 20 μM of the inhibitor, the relative HOCl-producing activity of MPO was even slightly higher than in the negative control. In contrast, starting at 50 μM of **28**, a constant drop in the relative chlorinating MPO activity was observed. At the highest tested inhibitor concentration

(1 mM), about 20 % of the original relative HOCl production was observed. Based on the obtained data, an IC_{50} value of about 93.1 μM was calculated (**Figure 12**).

For compound **42,** up to 50 μM of the inhibitor, no clear effect on the relative chlorinating MPO activity was observed. Yet at higher inhibitor concentration, a clear concentration-dependent decrease in the relative HOCl production rate was detected. At 2 mM of **42,** the relative MPO activity dropped to about 8.6 % of the value observed in the absence of the inhibitor. From the data, an IC_{50} value of about 313.6 μM was calculated (**Figure 12**).

ADME/T properties

Absorption, distribution, metabolism, excretion and toxicity (ADME/T) experimental properties of the most active compounds were obtained from admetSAR® (http://lmmd.ecust.edu.cn:8000/) database[40]. It is noteworthy that 4 selected compounds during the docking were drugs and were expected to be safe. However, in the absence of data, the properties were predicted using the same software. The predicted and experimental ADME/T properties of the active compounds are listed in **Table 6**. All the compounds can be absorbed from the intestinal tract as suggested by the LogP values ranging between 0.54 and 1.06 (**Table S6**). In addition, the toxicity values of our compounds are rather low possibly due to the OSIRIS filter which excluded the molecules with high risk of toxicity.

The *in vitro* growth inhibition of the active compounds in normal human dermal fibroblast (NHDF) was assessed by MTT assay to evaluate the potential cytotoxicity of the new inhibitors in a cellular model. The results are shown in **Table 6** and demonstrate that compound **28** inhibits the growth of these cells at a concentration (IC_{50}) of 17 μM, which is about 400 times higher than the concentration of the MPO inhibitory effect (0.044 μM). The other compounds do not seem to be cytotoxic, at least up until 50 μM (**Figure S6A**).

Furthermore, the effect of compounds **28** and **42** on the vitality of neutrophil was assessed. It is found that up to 1 mM, **28** did not significantly increase the apoptosis rate in the neutrophils. Still at concentrations of 500 μM or higher, the FSC/SSC plots indicate a small tendency for a higher necrosis rate in the cells (not shown). Again no significant effect of compound **42** on the apoptosis rate was observed in the tested concentration range (**Figure S6B**).

Effect of MPO inhibitors on lactoperoxidase

In order to assess the specificity, the activity of the potent compounds was also tested on lactoperoxidase (LPO) which is a homologous human peroxidase[41] (**Table 7**). Compounds **34**, **36** and **41** showed similar activity on both LPO and MPO, whereas compounds **28**, **60** and **42,** which represent the best irreversible and reversible inhibitors of MPO, showed a 100-times reduced activity on LPO.

Because of the small molecular weight of the active compounds, these might be active also on other targets (enzymes or receptors). The information obtained from PubChem database showed that **28** and its analogs have no activity on mammalian enzymes or receptors, however, on *Plasmodium falciparum* 3D7. Information about **39**, **42**, **45** and **55** activity on different targets is available in PubChem database (**Table S5**).

3. Discussion

The present study aimed at evaluating a new virtual screening approach consisting of ligand-based pharmacophore modeling and structure-based virtual screening in order to design new potent MPO inhibitors.

Four pharmacophore models were generated to screen a subset of the Zinc database containing compounds that match the Lipinski's rules. The pharmacophore model obtained

using **6** and **4** provided the largest pool of active molecules: 9 hits out of 15 tested compounds displayed IC_{50} less than 5 μM, five of them being active at nanomolar concentrations. According to the docking experiment, this model highlighted the specific interactions of each candidate with the active site. The ionizable basic groups in both **6** and **4** form the same interaction in the active site, i.e. a salt bridge with Glu102. In addition, their aromatic groups form π-π interactions with the heme. The presence of these two types of interaction may explain the success of pharmacophore model 1 as the other 3 models do not feature aromatic and amine groups in both compounds. Furthermore, the HBD or HBA functions of the potent inhibitors exhibit a different interaction with the enzyme (i.e. the HBD of **6** and **7** forms hydrogen bond with Glu102, while that of **1** faces the heme iron). This observation could be rationalized by considering that the HBD group in **1** contained in a hydroxamic acid group that is known to have an excellent affinity for heavy metals such as iron, whereas the amino group of **6** and the amide group of **7** do not possess this property.

All the ligands issued from our protocol share an aromatic ring, a HBA on the aromatic group and a HBD or a positively charged group at the alkyl chain. Following the docked poses, the aromatic moiety of most ligands is involved in a π-stacking with the pyrrole D of the heme, and their positively charged group or HBD interacts with Glu102. Noticeably several compounds selected from the virtual docking based on their scoring values showed a low activity and some of them even had none (i.e. **29**, **30**, **38**, **40**, **44**, **46**, **47, 49** and **51**). Other compounds such as serotonin[7] and 5-carboxytryptamine[29] were also previously reported to be inactive despite their good affinity[9]. These observations were explained by prevailing weaknesses of the scoring function used in the docking programs to estimate the experimental affinities[19]. This is indeed observed here as the ΔG score values and the activity of the inhibitors correlate poorly. Another possible cause for this poor correlation found for some compounds could be rationalized by their potential to react with MPO which cannot be

modeled by the docking. Despite these weaknesses, our procedure produced 21 active out of 24 tested compounds (88%), and 12 had an IC_{50} less than 5 μM (50%).

A kinetic study based on active (**28, 36** and **43**) and inactive (**40** and **29**) ligands was carried out in order to understand the mechanism of inhibition of the active inhibitors and the absence of activity of the others. In general, a compound is endowed with a high activity when it is able to react fast with Compound I and slowly with Compound II leading to the accumulation of Compound II which does not participate in the halogenation cycle ($k_3>>k_4$)[7, 27]. This classical phenomenon was found for **43** (**Figure 9A** and **B**)(Table 3).

Initially, also oxidation of **28** and **36** follows the classical peroxidase cycle. Both molecules are oxidized by Compounds I and II, however, the resulting reaction products (i.e. radicals) apparently shift the enzyme out of the peroxidase cycle into the Compound III state. Normally, the latter can only be formed from ferric or ferrous MPO with superoxide (k_6) or dioxygen (k_7) respectively (**Figure 1**). It seems that the substrate radicals react with ferric MPO and reduce it to ferrous enzyme (k_5) or alternatively, reduce dioxygen to superoxide that reacts with ferric MPO to Compound III. Only partial recovery of ferric MPO after H_2O_2 consumption demonstrated that these molecules are mechanism-based inhibitors since they irreversibly inhibited MPO in a H_2O_2-dependent reaction. Irreversible inhibition was also seen in peroxidase activity assays in the presence of competing electron donors like guaiacol. Complete inhibition of MPO by **28** and **36** is achieved by a [inhibitor]/[MPO] ratio of 67 and 110, respectively. In contrast, all other tested inhibitors showed a completely different behavior, i.e. they followed the peroxidase cycle and their inhibitory activity did not depend on the presence of hydrogen peroxide.

In the case of **40**, the values of k_3 and k_4 did not show a sufficient k_3/k_4 ratio to promote accumulation of Compound II and as a result the ligand has no activity. **29** slowly reacts with

Compound I (k_3 at the order of 10^4 $M^{-1}s^{-1}$), and consequently, cannot compete with the natural electron donor, chloride anion. Thus, our kinetic results showed that the inactive compounds selected by our screening method either react in a very fast way with both Compound I or II or are poor substrates of MPO. This indicates that a potent MPO inhibitor must be a good electron donor for Compound I capable of shifting the activity of the enzyme to the peroxidation cycle. In some cases, the subsequent products of this reaction further react with the redox intermediates of MPO to irreversibly block the enzyme as **28** and **36** do.

In general, predictions of biological activities based on docking experiments are below 50% for most of the tested enzymes[42]. For MPO, this was shown to drop to 10%[20]. Our study suggests that the ligand-based pharmacophore modeling may contribute to improving the results (50% with our procedure versus 10% with structure-based virtual screening), especially when model 1 is used due to the similarity of the chemical and physiochemical properties of both tested inhibitors (**6** and **4**). It has been demonstrated that the compound must have one oxidable group in order to promote Compound II formation[43]. Ligand-based pharmacophore modeling may contribute in selecting compounds with such groups. Malvezzi et al used also ligand-based pharmacophore modeling as a virtual screening procedure to find new MPO inhibitors. However, they used only SHA as a pharmacophore model and discovered nine compounds derived from phenylhydrazide (4 compounds with IC_{50} < 5 μM)[20]. Despite the fact that the hit rate of their virtual screening was high compared to structure-based virtual screening[20], all were derived from the same scaffold. Notably, to reach the heme cavity of MPO, compounds have to go through a rather narrow channel lined with hydrophobic patches. In that respect, our procedure which included a Lipinski's rule filter may have improved the results by selecting the compounds that have suitable molecular mass and lipophilicity.

It has been documented that MPO-dependent LDL oxidation plays an important role in atherogenesis. In addition, there are numerous pieces of evidence that the complex of MPO with ApoB-100 of LDL is mainly formed through electrostatic interactions and modifies the chemical and steric requirements for efficient penetration of substrates and/or inhibitors into the binding site[41]. In this context, the inhibiting potency of the new inhibitors on LDL oxidation carried out by the MPO/H_2O_2/Cl^- system has been assessed. The results demonstrated that the compounds with IC_{50} > 5 μM cannot inhibit the oxidation of LDL carried out by MPO. This decrease in inhibitory activity in the LDL assay compared to the taurine test may be caused by the hindrance of the catalytic site during binding to LDL, thereby providing some protective effect[42]. The heme group of MPO that is responsible for the enzymatic activity is indeed located in a distal hydrophobic cavity with a narrow oval-shaped opening. Hence, the formation of a complex macromolecular structure between MPO and LDL may modify the chemical and steric requirements for good penetration of substrates and/or inhibitors into the heme cavity[45]. Parameters such as charge and lipophilicity of compounds have already been evoked to explain similar results[19].

The molecular meachanism of modification of MPO by **36** and **28** remains elusive. Upon oxidation by Compounds I and II both molecules are oxidized to radicals. In the case of **36**, the primary amine is oxidized[38] followed by transfer of the radical site to the aromatic ring and loss of the diamino group. Then, either the resulting intermediate loses another electron, forming a stable phtalazine, or might react with the heme group leading to irreversible modification and inhibition of MPO (**Figure 13A**). A similar oxidation pathway can be proposed for **28.** The corresponding one-electron oxidation product could lose one amino group or a diamine-methylene group forming two radical intermediates which in turn react with the heme or lose another electron to give stable molecules (**Figure 13B**).

In order to further optimize the activity of **28** (the best hit and the mechanism-based inhibitor) several derivatives were synthesized and tested. The results showed that a halogen atom on the aromatic ring is very important for the inhibitory activity. According to docking, this group features a hydrogen bond with His95 and/or Gln91 (**Figure 11**). However, this interaction is achieved only when the HBA is on the position 7 of the quinazoline. In addition, the activity increase follows the hierarchy F > Cl > Br. This can be explained by an increase of the volume from F to Br and/or increasing the electronegativity from Br to F.

Of course inhibition of MPO might dampen the antimicrobial activity of MPO during phagocytosis of neutrophils. In fact, the effects of compounds **28** and **42** on human neutrophils indicate that these compounds also efficiently inhibit intracellular MPO. Yet the almost 10^4- and 10^5-times higher IC_{50} values for compounds **28** and **42** strongly indicate a much weaker effect on intracellular MPO than on the extracellular enzyme, maybe due to restricted membrane permeability. Thus these two inhibitors have only limited effect on the antimicrobial activity of neutrophils.

The predicted and experimental ADME/T profiles and the selectivity in other peroxidases of the new inhibitors make these molecules promising hits. Four of these inhibitors are commercially available drugs with known ADME/T profiles. Compound **43** which is commonly used to treat and prevent nausea and vomiting has an IC_{50} of 0.35 μM on MPO. It has been demonstrated that the plasma level of this safe drug (pregnancy category: B) after one treating oral dose is 0.2-0.4 μM which is of the same order as its MPO[46]. In addition, it is found that MPO inhibitors may be useful in cardiovascular diseases (CVD). Ruggeri et al reported that compound **12** is useful for treatment of CVD[34]. However, it is found in this study that **36**, used for CVD in the cases of high blood pressure and heart failure, has an activity 2-times higher than **12**. The concentration of **36** in plasma after one oral dose was found to be 3.8-6.7 μM which corresponds to its IC_{50} value on MPO activity[47].

4. Conclusion

In summary, 12 active MPO inhibitors were identified. Most of them act simply as electron donors toward this important oxidoreductase, blocking efficiently and reversibly its halogenation activity. Compound **28** was found to be a mechanism-based inhibitor of high inhibitory potency. It is oxidized by the relevant enzymatic redox intermediates Compounds I and Compound II to the corresponding one-electron oxidation products that attack the enzyme and irreversibly modify its structure. Actually, **28** and **4** are the first mechanism-based inhibitors which inhibit MPO at nanomolar concentration. By pharmacomodulation, further active compounds were obtained. This approach of combining ligand-based pharmacophore modeling and structure-based virtual screening seems to be promising to obtain new scaffolds of MPO inhibitors.

5. Experimental Section:

Synthesis

^{1}H- and ^{13}C-NMR spectra were taken on a Bruker Avance 300 MHz spectrometer (Wissemburg, France) at 293 K. Chemical shifts (δ) are given in parts per million (ppm) relative to DMSO-d_6 or $CDCl_3$, and the coupling constants are expressed in hertz. Infrared spectroscopic analysis was performed with a Shimadzu (Kyoto, Japan) IRAffinity-1 spectrophotometer equipped with an ATR device, and the peak data are given in cm^{-1}. All reactions were followed by thin-layer chromatography (TLC) carried out on Fluka (Bornem, Belgium) PET foils silica gel 60, and compounds were visualized by UV. Column chromatographies were performed with EchoChrom MP silica 63-200 from MP Biomedicals (Santa Ana, CA). Organic solutions were dried over Na_2SO_4 and concentrated with a Buchi rotatory evaporator (Flawil, Switzerland). Starting materials aniline, 4-chloroaniline, 3-chloroaniline, 4-bromoaniline, 3-bromoaniline and 4-(trifluoromethyl)aniline were available

from TCI (Japan). 1-Cyanoguanidine was purchased from Sigma-Aldrich (Bornem, Belgium). Purity was determined by liquid chromatography (LC) with diode-array detection (DAD) (Agilent) on a 150 mm × 4.6 mm Symmetry C18 column at a mobile phase flow rate of 1 mL/min. The mobile phase was a mixture of methanol (350 mL) and a KH_2PO_4 solution (0.07 M in water, 650 mL) adjusted to pH 3.0 with a 34 wt % H_3PO_4 solution. The chromatograms were extracted at maximum absorption wavelengths by using the Max Plot extraction mode. The purity was ≥ 95% for all compounds.

General procedure of synthesis of N-(4-methylquinazoline-2-yl)-guanidine derivatives[39]

To a solution of aniline derivative (10 mmol) in freshly distilled acetone (17 mL) was added iodine (1.0 g, 4 mmol). The resultant solution was heated to 130 °C for 2 days. The solution was cooled to room temperature and concentrated in vacuo. The residue was dissolved in dichloromethane, washed with a 5% sodium bicarbonate and with brine. The solvent removed in vacuo to give 2.0 g of brown oil. Purification on silica gel via flash column chromatography (ethyl ether/ petroleum ether 3:97) gave 1,2-dihydro-2,2,4-trimethylquinoline derivatives. The resulting compound (1 mmol) was dissolved in dry acetonitrile (0.4 mL) and added to a solution of hydrochloric acid in diethylether (2 M, 1 mL, 2 mmol). The resultant solution was stirred at room temperature until precipitation. The brown crystals were filtered, washed with dry hexane and dried in vacuo. The hydrochloride salt (0.9 mmol) was suspended in a mixture of water (1.5 mL) and EtOH (1 mL), and dicyandiamide (75 mg, 0.9 mmol) was added. The resultant solution was refluxed for 1 day, and then decanted hot, removing the brown oil that formed during the reaction. The solution was adjusted to pH 10-11 with 2M potassium hydroxide and concentrated in vacuo until a precipitate began to form. The solution was then filtered and the precipitate washed with cold water. The cured compound was suspended in chloroform by the aid of sonicator. Then the suspension was filtered and the precipitate washed with chloroform.

N-(4-Methyl-quinazolin-2-yl)-guanidine (56)

The titled compound was synthesized according to the general procedure to give a yellowish solid (40 mg, 20% yield). ^{1}H NMR (DMSO-d_6) δ 8.06 (d, 1H, J = 9 Hz, H-8), 7.93 (t, J= 3 Hz, 1H, H-7), 7.90 (t, 1H, J= 3 Hz, H-6), 7.67 (d, 1H, J = 9 Hz, H-5), 2.94 (s, 3H, CH_3). ^{13}C NMR (DMSO-d_6) δ 159.5 (C-guanidine*), 157.3 (C-2*), 155.3 (C-4), 148.8 (C-8a), 135.2 (C-7), 128.7 (C-8), 127.4 (C-6), 126.8 (C-5), 125.3 (C-4a), 21.9 (CH_3). IR (FT) 3325, 3143, 2197, 2150, 1622, 1503, 1333, 1248, 1026, 927 cm^{-1}.

N-(6-Fluoro-4-methyl-quinazolin-2-yl)-guanidine (57)

The titled compound was synthesized according to the general procedure to give a yellowish solid (37 mg, 17% yield). ^{1}H NMR (DMSO-d_6) δ 8.17 (ddd, 1H, J = 9, 9, 3 Hz, H-7), 8.03 (dd, 1H, J = 9, 4 Hz, H-8), 7.94 (dd, 1H, J = 9, 3 Hz, H-5), 2.83 (s, 3H, CH_3). ^{13}C NMR (DMSO-d_6) δ 167.4 (d, J= 233 Hz, C-6), 158.9 (C-guanidine*), 157.9 (C-2*), 153.1 (C-4), 150.3 (C-8a), 136.2 (d, J= 18.9 Hz, C-7), 132.2 (d, J = 20 Hz, C-5), 130.6 (d, J = 7 Hz, C-8), 126.5 (C-4a), 22.7 (CH_3). IR (FT) 3325, 3143, 2197, 2150, 1622, 1503, 1333, 1248, 1026, 927 cm^{-1}.

N-(6-Chloro-4-methyl-quinazolin-2-yl)-guanidine (58)

The titled compound was synthesized according to the general procedure to give a yellowish solid (84 mg, 36% yield). ^{1}H NMR (DMSO-d_6) δ 8.22 (d, 1H, J = 9 Hz, H-8), 7.86 (m, 2H, H-5, 7), 2.95 (s, 3H, CH_3). ^{13}C NMR (DMSO-d_6) δ 158.6 (C-guanidine*), 157.1 (C-2*), 155.0 (C-4), 148.6 (C-8a), 136.4 (C-7), 132.4 (C-6), 130.6 (C-8*), 129.1 (C-5*), 123.9 (C-4a), 21.4 (CH_3). IR (FT) 3325, 3143, 2197, 2150, 1622, 1503, 1333, 1248, 1026, 927 cm^{-1}.

N-(6-Bromo-4-methyl-quinazolin-2-yl)-guanidine (59)

The titled compound was synthesized according to the general procedure to give a yellowish solid (59 mg, 21% yield). ^{1}H NMR (DMSO-d_6) δ 8.40 (d, J = 3 Hz, 1H, H-5), 7.99 (dd, J = 9, 3 Hz, 1H, H-7), 7.85 (d, J= 9 Hz, 1H, H-8), 2.93 (s, 3H); IR (FT) 3325, 3143, 2197, 2150, 1622, 1503, 1333, 1248, 1026, 927 cm^{-1}.

N-(7-Fluoro-4-methyl-quinazolin-2-yl)-guanidine (60)

The titled compound was synthesized according to the general procedure to give a yellowish solid (37 mg, 17% yield). ^{1}H NMR ($CDCl_3$) δ 7.31 (dd, 1H, J = 9, 6 Hz, H-5), 7.23 (dd, 1H, J = 9, 3 Hz, H-8), 6.97 (ddd, 1H, J = 9, 9, 3 Hz, H-6), 5.19 (s, 4H, $2NH_2$), 2.05 (s, 3H, CH_3). ^{13}C NMR ($CDCl_3$) δ 160.6 (d, J= 143 Hz, C-7), 157.7 (C-guanidine*), 156.6 (C-2*), 133.3 (C-4), 127.7 (d, J= 7 Hz, C-8a), 114.2 (d, J = 6 Hz, C-4a), 112.3 (d, J = 10 Hz, C-5), 110.9 (d, J = 26 Hz, C-6), 103.9 (d, J = 23 Hz, C-8), 24.3 (CH_3). IR (FT) 3325, 3143, 2197, 2150, 1622, 1503, 1333, 1248, 1026, 927 cm^{-1}.

N-(7-Chloro-4-methyl-quinazolin-2-yl)-guanidine (61)

The titled compound was synthesized according to the general procedure to give a yellowish solid (56 mg, 24% yield). ^{1}H NMR (DMSO-d_6) δ 8.27(d, J = 9Hz, 1H, H-5), 8.19 (s, 1H, H-8), 7.78 (d, J = 9 Hz, 1H, H-6), 2.99 (s, 3H); ^{13}C NMR (DMSO-d_6) δ 159.9(C-2*), 157.9 (C-guanidine*), 151.7 (C-4), 149.7 (C-8a), 136.5 (C-7), 132.6 (C-8), 131.3 (C-6), 127.9 (C-5), 125.4 (C-4a), 21.9 (CH_3). IR (FT) 3325, 3143, 2197, 2150, 1622, 1503, 1333, 1248, 1026, 927 cm^{-1}.

N-(7-Bromo-4-methyl-quinazolin-2-yl)-guanidine (62)

The titled compound was synthesized according to the general procedure to give a yellowish solid (42 mg, 15% yield). ^{1}H NMR (DMSO-d_6) δ 8.09 (d, J = 9 Hz, 1H, H-6), 7.89 (s,1H, H-8), 7.68 (d, J = 9 Hz, 1H, H-5), 2.93 (s, 3H); ^{13}C NMR (DMSO-d_6) δ 159.1(C-2*), 157.5 (C-

guanidine*), 153.5 (C-4), 150.7 (C-8a), 134.2 (C-8), 130.8 (C-6), 128.5 (C-7), 127.2 (C-5), 126.0 (C-4a), 22.4 (CH_3). IR (FT) 3325, 3143, 2197, 2150, 1622, 1503, 1333, 1248, 1026, 927 cm^{-1}.

Data Sets

For the virtual screening campaigns, the ZINC database v.8 was downloaded from the ZINC Web site (http://zinc.docking.org/). This database is composed of 727842 small synthetic chemicals and consists of compounds. These compounds were transformed into a LigandScout ® database using the idbgen-tool of LigandScout®. The selected compounds (Zinc codes of these compounds are available in Table S1) were purchased from Aurora Fine Chemicals Ltd. The remaining selected compounds were available from Fagron (Belgium).

Pharmacophore Modeling

DruLiTo software (ref: http://www.niper.gov.in/pi_dev_tools/DruLiToWeb/DruLiTo_index.html) was used to filter the Zinc database molecules against the Lipinski's rules that is the selected molecules have no more than 5 hydrogen bond donors and 10 hydrogen bond acceptors, a molecular mass less than 500 g mol^{-1} and a Moriguchi's logP (MLogP) < 5.

The pharmacophore models were constructed using LigandScout®3.12 (www.inteligand.com). In a shared feature pharmacophore model generation, LigandScout generates pharmacophore models from the chemical functionalities of the training compounds and aligns the molecules according to their pharmacophores. In our study, the search for a pharmacophore using the structural data of all seven highly potent MPO inhibitory compounds (**Figure 2**) was not successful. The models obtained using each of the seven inhibitors selected only compounds analogous to this inhibitor (so no new scaffold was found). The search made combining the seven inhibitors per different groups of three

molecules selected very large ensembles of hits because of the low numbers of the shared functional groups. Only the models obtained using the seven inhibitors in pairs produced pharmacophores with the highest number of shared chemical functionalities.

The quality of the pharmacophore models was quantitatively evaluated by calculating the selectivity (eq 1) and specificity (eq 2) for each model using known active and inactive compounds.

Eq1 $$\text{selectivity} = \frac{\text{found active}}{\text{all the tested compounds}}$$

Eq2 $$\text{specificity} = \frac{\text{found inactive}}{\text{all the tested compounds}}$$

Docking experiments

Docking was performed with FlexX program included in LeadIT (version 2.1.8) or with the Glide program (version 7.4).

The X-ray structure of human myeloperoxidase complexed to thiocyanate (PDB code 1DNU) was used as the target structure for the docking studies with FlexX[16]. The protein dimer was loaded into LeadIT ® 2.1.8 and chains B and D were selected to form the receptor components. The binding site was defined by choosing thiocyanate as a reference. Amino acids within 11 Å of the ligand were selected as binding site (the residues 81 to 120 and 330 to 337). The X-ray water and other ligand molecules were removed from the active site. The ligand input files were prepared according to the following procedure. The initial 3D structures of the ligands were generated by use of the LigandScout ® procedure[48]. The prediction of different protonation states of all ligands was achieved with the protonation state option in LeadIT ® software. For the stereochemistry, the options R/S and pseudo R/S were chosen in stereo mode to cover all the possible stereo models of the ligands. Docking was performed with FlexX program included in LeadIT (version 2.1.8), no additive filters were

applied. Hydrogen bond donors and acceptors, phenyl centers, and hydrophobic features are defined similarly in FlexX as pharmacophore features. The FlexX scoring function was used. The ligand binding was driven by hybrid approach (enthalpy and entropy). The remaining parameters were set to their default values. The experiment was validated using the crystal **1** ligand[49-50].

The X-ray structure of human MPO complexed to compound **1** (PDB code 4C1M) was used as the receptor targets in docking studies[51]. The X-ray water and other ligand molecules were removed from the active site. The initial 3D structures of the ligands were generated with the Ligprep module (Schrodinger, LLC, New York, NY, 2017) and the ligand partial charges were ascribed by use of the OPLS force field. The Epik program was used to predict different protonation states of all ligands[52]. The Glide XP docking protocol and scoring function were used. The remaining parameters were set to their default values.

In Silico Toxicological Evaluation and Drug-Like Profile

The in silico toxicity and drug-like profile of the selected molecules were calculated using the Program OSIRIS Property Explorer. Data were generated on-line in the Osiris Program, accessed by the link (http://www.organic-chemistry.org/prog/peo/) and represented by toxicity risks (mutagenic, irritant, tumorigenic and reproductive effects), drug likeness and drug-score. Drug likeness was calculated based on equation summing up score values of the fragments present in the molecule under investigation. The fragments were identified from a list of 5,300 distinct substructure fragments with associated drug likeness scores. Drug-score was calculated combining the drug likeness, cLogP, logS, molecular weight and toxicity risks data. The compound was selected when all the following criteria were achieved: no tumorigenicity risk, no reproductive effect risk, no mutagenicity risk, no irritating effect risk, drug-likeness $\leq$-0.05, and drug-score $\geq$0.5.

Enzymatic Activity Assays

Taurine Chlorination Assay

The assay is based on the production of taurine chloramine produced by the MPO/H_2O_2/Cl^- system in the presence of a selected inhibitor at defined concentration. The reaction mixture contained the following reagents in a final volume of 200 μL: 10 mM phosphate buffer (pH 7.4, 300 mM NaCl), 15 mM taurine, compound to be tested (up to 20 μM), and a fixed amount of recombinant MPO (6.6 μL of MPO batch solution diluted 2.5 times, 40 nM). When necessary, the volume was adjusted with water. This mixture was incubated at 37 °C and the reaction was initiated with 10.0 μL of H_2O_2 (100 μM). After 5 min, the reaction was stopped by the addition of 10 μL of catalase (8 units/μL). To determine the amount of taurine chloramine produced, 50 μL of 1.35 mM solution of thionitrobenzoic acid was added and the volume was adjusted to 300 μL with water. Then the absorbance of the solutions was measured at 412 nm with a microplate reader, and the curve of absorbance as a function of inhibitor concentration was plotted. IC_{50} values were then determined by standard procedures, taking into account the absence of hydrogen peroxide as 100% inhibition and the absence of inhibitors as 0% inhibition[19].

Mechanism of MPO inhibition

The respective compound (5 μM) was incubated with 100 nM MPO in 100 mM phosphate buffer, pH 7.4, at 21 °C with or without 30 μM hydrogen peroxide in the absence or presence of 100 mM sodium chloride. Five minutes after adding hydrogen peroxide to start the reaction, the enzyme was diluted 100-fold, and its residual peroxidation activity was measured using 3,3′,5,5′-tetramethylbenzidine (TMB) as the peroxidase substrate.

In order to probe the binding of the potential inhibitors at the active site of MPO, 50 nM MPO was incubated in 10 mM phosphate buffer (pH 7.4, 300 μM NaCl) with 5 μM of the inhibitor

and 30 μM TMB with or without 10 μM tyrosine. After 5 min, 10 μM H_2O_2 was added, and then the MPO activity was immediately monitored at 470 nm during 10 minutes (Agilent spectrophotometer 8543).

Transient-State Kinetics

Highly purified myeloperoxidase with purity index (A_{430}/A_{280}) of at least 0.86 was purchased from Planta Natural Products (http://www.planta.at). Its concentration was calculated by use of ε_{430} = 91 $mM^{-1}\cdot cm^{-1}$. Hydrogen peroxide obtained from a 30% solution was diluted and the concentration was determined by absorbance measurement at 240 nm, where the extinction coefficient is 39.4 $M^{-1}\cdot cm^{-1}$. Tested compounds stock solutions were prepared in dimethyl sulfoxide (DMSO) and stored in dark flasks. Dilution was performed with 200 mM phosphate buffer, pH 7.4, to a final DMSO concentration of 2% (v/v) in all assays.

The multimixing stopped-flow measurements were performed with the Applied Photophysics (UK) instrument SX-18MV. When 100 μL was shot into a flow cell having a 1 cm light path, the fastest time for mixing two solutions and recording the first data point was 1.3 ms. Kinetics were followed both at single wavelength and by use of a diode-array detector. At least three determinations (2000 data points) of pseudo-first-order rate constants (k_{obs}) were performed for each substrate concentration (pH 7.4, 25 °C) and the mean value was used in the calculation of the second-order rate constants, which were calculated from the slope of the line defined by a plot of k_{obs} versus substrate concentration. To allow calculation of pseudo-first-order rates, the concentrations of substrates were at least 5 times in excess of the enzyme.

Conditions of MPO compound I formation were described by Furtmüller *et al*[50]. Typically, 8 μM MPO was premixed with 80 μM H_2O_2, and after a delay time of 20 ms, compound I was allowed to react with varying concentrations of the tested compounds in 200 mM phosphate buffer, pH 7.4. The reactions were followed at the Soret maximum of Compound II (456 nm).

Compound II formation and reduction could be followed in one measurement. The resulting biphasic curves at 456 nm showed the initial formation of Compound II and its subsequent reduction to native MPO by the tested compounds (decrease in absorbance at 456 nm).

Residual MPO activity

To determine the partition ratio for **28** and **36**, MPO (50 nM) in 10 mM phosphate buffer (pH 7.4) was incubated with 2 μM H_2O_2 and the inhibitor at concentrations ranging from 0.05 to 20 μM to achieve varying ratios of [inhibitor]/[MPO]. After 15 min, an aliquot of the preincubation mixture was rapidly diluted 100-fold into the assay buffer containing 2 μM H_2O_2 and 30 μM 3,3′,5,5′-tetramethylbenzidine (TMB). The peroxidase activity of MPO was determined from the initial slope of the corresponding time traces. Finally, the fractional MPO activity was plotted as a function of the [inhibitor]/[MPO]ratio.

Determination of LDL Oxidation Inhibition

Preparation of the Recombinant Enzyme and of LDL

Recombinant MPO was prepared as previously described[53]. Each batch solution is characterized by its protein concentration (mg/mL), its activity (U/mL), and its specific activity (U/mg). The chlorination activity was determined according to Hewson and Hager[54]. Human plasma served for the isolation of LDL by ultracentrifugation according to Havel *et al.*[55]. Before oxidation, the LDL fraction ($1.019 < d < 1.067$ g/mL) was desalted by two consecutive passages through PD10 gel-filtration columns (Amersham Biosciences, The Netherlands) using PBS buffer. The different steps were carried out in the dark, and the protein concentration was measured by the Lowry assay for both MPO and LDL.

Inhibition of LDL Oxidation

LDL oxidation was carried out at 37 °C in a final volume of 500 µL. The reaction mixture contained the following reagents at the final concentrations indicated between brackets: pH 7.2, PBS buffer, MPO (1 µg/mL), LDL (1000 µg/mL), 2 µL 1 N HCl (4 mM), one of the drugs at different concentrations, and H_2O_2 (100 µM). The reaction was stopped after 5 min by cooling the tubes in ice. The assay was performed in a NUNC maxisorp plate (VWR, Zaventem, Belgium): 200 ng/well of LDL was coated overnight at 4 °C in a sodium bicarbonate pH 9.8 buffer (100 µL). Afterward, the plate was washed with TBS 80 buffer and then saturated during 1 h at 37 °C with the PBS buffer containing 1% BSA (150 µL/well). After washing the wells twice with the TBS 80 buffer, the monoclonal antibody Mab AG9 (200 ng/well) obtained according to a standard protocol and as previously described was added as a diluted solution in PBS buffer with 0.5% BSA and 0.1% of Polysorbate 20. After incubation for 1 h at 37 °C, the plate was washed four times with the TBS 80 buffer and a 3000 times diluted solution of IgG antimouse alkaline phosphatase (Promega, Leiden, The Netherlands) in the same buffer was added (100 µL/well). The wells were washed again four times and a revelation solution (150 µL/well) containing 5 mg of *para*-nitrophenyl phosphate in 5 mL of diethanolamine buffer was added for 30 min at room temperature. The reaction was stopped with 60 µL/well of 3 N NaOH solution. The measurement of the absorbance was performed at 405 nm with a background correction at 655 nm with a Bio-Rad photometer for a 96-well plate (Bio-Rad laboratories, CA, USA). Results were expressed as IC_{50}[56].

Assessment of LPO activity

The reaction mixture for the LPO activity assay contained the following reagents in a final volume of 200 µL: 10 mM phosphate buffer (pH 7.4, 300 mM NaSCN), compound to be tested (0.1, 0.5, 1, and 5 µM), and a fixed amount of LPO (LPO, obtained from Sigma-Aldrich, Taufkirchen, Germany, 10 µL). When necessary, the volume was adjusted with water. This mixture was incubated at 37 °C and the reaction was initiated with 10.0 µL of

H_2O_2 (100 μM). After 5 min, the reaction was stopped by the addition of 10 μL of catalase (8 units/μL). To determine the amount of NaOSCN produced, 50 μL of 1.35 mM solution of thionitrobenzoic acid was added and the volume was adjusted to 300 μL with water. Then the absorbance of the solutions was measured at 412 nm with a microplate reader, and the curve of absorbance as a function of inhibitor concentration was plotted. IC_{50} values were then determined by standard procedures, taking into account the absence of hydrogen peroxide as 100% inhibition and the absence of inhibitors as 0% inhibition[57].

Characterization of the oxidation products of 36 and 28

The irreversible inhibitor (4 μM) was incubated with 100 nM MPO in 10 mM phosphate buffer (pH 7.4, 300 mM NaCl). This mixture was incubated at 37 °C and the reaction was initiated with 10.0 μL of H_2O_2 (100 μM). After 60 min, the mixture was injected to LC-MS. Mass spectrometric data were obtained on a QTOF 6520 (Agilent, Palo Alto, CA), column Zorbax C18, positive mode, min range (m/z) 50, max range (m/z) 1050, scan rate 1 / sec, by diffusion of 0.2 mL/min and pressure 550 bar, by mobile phase HCOOH (0.1% in water)/ HCOOH 0.1% in CH_3OH (gradient mode as following: 0 min, 1% solvent B; 3 min, 5% solvent B; 15 min, 90% solvent B; 25 min, 90% solvent B; 25.5 min, 5% solvent B; 30 min, 5% solvent B) (VCAP 3500 V, source T, 350 °C; fragmentation, 110 V; skimmer, 65 V).

Evaluation of the impact of potential inhibitors on the cell growth

In order to evaluate whether selected compounds (**28**, **34**, **36**, **39**, **41**, **42**, **43** and **55**) exhibited toxicity at the cellular level at concentrations ranging from 0.005 to 50 μM, the colorimetric assay MTT was performed[58] in Normal Human Dermal Fibroblasts (NHDF, Lonza CC-2509). Briefly, cell line was cultured in cell culture flasks, grown and maintained at 37 °C, 95% humidity, 5% CO_2 in fibroblast medium FBM (Lonza, Walkersville, USA) supplemented with 2% fetal bovine serum, 0.1% insulin, rhFGF-B and gentamicin and amphotericin. NHDF cells

were chemically detached with trypsin and seeded in 96 well plates and left to attach for 24 h. Prior to treatment, compounds were dissolved in DMSO at a concentration of 10 mM and cells were treated with the different concentrations of the compounds diluted in culture medium (5 nM to 50 μM) or left untreated for 72 h. The amount of viable cells was determined through the MTT (3-(4,5-dimethylthiazol-2-yl)-2,5-diphenyltetrazolium bromide; Sigma, Bornem, Belgium) mitochondrial reduction into formazan by living cells, according to previously described[58]. The optical density (O.D.) was measured in a Biorad 680RX plate reader (Biorad, Nazareth, Belgium) at 570 nm (reference 630 nm) and the O.D. of the untreated control was normalized as 100% of viable cells, allowing determination of the concentration that inhibited their growth by 50% (IC_{50}).

Evaluation of the impact of potential inhibitors on human neutrophils

All chemicals used for the isolation and staining of neutrophils (polymorphonuclear leukocytes, PMNs) were obtained from Sigma-Aldrich, Taufkirchen, Germany. Exceptions are the Biocoll solution purchased from Biochrom AG, Berlin, Germany and aminophenyl fluorescein (APF) obtained from Cayman Chemical Company, Ann Arbor, MI, USA.

The *ex vivo* testing of selected MPO inhibitors was performed on purified human neutrophils. Thereby the cells were isolated from heparinized peripheral human blood of healthy volunteers by using a well-established protocol[59]. Briefly, erythrocytes and other leukocytes were removed by subsequently applying dextran-enhanced sedimentation, Biocoll density gradient centrifugation and hypotonic lysis. Afterwards the cells were diluted in Ca-containing HBSS at a concentration of 10^6 PMNs/mL and incubated with the inhibitors for 30 min at 37 °C, 95 % humidity, and 5 % CO_2. The cells were incubated with up to 1 mM of the compounds, which corresponds to a maximal final methanol concentration of 1 %. Some samples were incubated with 1 mM of the well-known MPO inhibitor 4-aminobenzoic acid hydrazide (4-ABAH)[60].

After incubation the samples were split and subjected to vitality as well as to MPO activity staining, respectively. Briefly, the apoptosis rate in the samples was addressed by applying the dye 5,5′,6,6′-tetrachloro-1,1′,3,3′-tetraethylbenzimidazolylcarbo-cyanine iodide (JC-1). Thereby the staining protocol of the supplier was applied with minor modifications[61]. As a positive control, one sample was stained in the additional presence of valinomycin. For the determination of the chlorinating MPO activity again a well-established protocol was applied[62]. Briefly, the samples were stained with 20 µM APF and 500 µM H_2O_2. Regarding the latter the concentration of the working solution was determined spectroscopically at 230 nm ($\varepsilon_{230} = 74\ M^{-1}\ cm^{-1}$)[63] by using a Cary60 UV-Vis spectrometer from Agilent Technologies, Waldbronn, Germany. All flow cytometry measurements were performed on a BD Accuri C6 Flow Cytometer, BD Germany, Heidelberg, Germany.

Determination of LogP values

Ten mg of the tested compound were dissolved in 10 mL n-octanol and 10 mL water. After shaking for 1 min the concentrations of the compound were measured in the organic and aqueous phases by spectrophotometer (SHIMADZU UV-1800). LogP was calculated as following:

$$\text{LogP} = Log(\frac{C_{octanol}}{C_{water}})$$

Supporting Information

Docking figures for all compounds, spectral analyses of the synthetic compounds, purity data for the commercial compounds, physiochemical properties of the synthetic, PubChem properties, comparing of the docking poses FlexX and Glide (Table and figures), comparing of the docking poses in normal and mutated MPO (Figures), molecular formula strings and

zinc codes of the compounds. This material is available free of charge via the Internet at http://pubs.acs.org.

Accession Codes

The PDB code for MPO is 1DNU.

Acknowledgment

This study was supported by Grant 34553.08 from the Belgian Fund for Scientific Research (FRS-FNRS), a grant from FER 2007 (ULB), and a grant from the Department of International Relationship (BRIC 2007). M.P. is a Senior Research Associate at the FRS-FNRS (Belgium). We thank "Wallonie Bruxelles International" Agency (www.wbi.be). We thank also Biosolveit® (www.biosolveit.de) and LigandScou® (www.rsc.org/chemistryworld/Issues/2006/September/LigandScout.asp). Dr. Jalal Soubhye is a research fellow of the FRS-FNRS.

The authors declare no competing financial interest.

Abbreviations Used

MPO, Myeloperoxidase; LDL, Low density lipoprotein; HDL, High density lipoprotein; SAR, Structure activity relationship; HBA, Hydrogen bond acceptor; HBD, Hydrogen bond donor; H, Hydrophobic feature; H, PI, Positively charge group; XVOL, Exclusion volume; CVD, Cardiovascular diseases.

***Corresponding Authors**

Jalal Soubhye: E-mail: jsoubhye@ulb.ac.be; phone: +32-2-650.52.89.

Francois Dufrasne: E-mail: dufrasne@ulb.ac.be; phone: +32-2-650.52.35.

Pierre Van Antwerpen: E-mail: pvantwer@ulb.ac.be; phone: +32-2-650.52.49.

§ **Author Contributions**

François Dufrasne and Pierre Van Antwerpen are authors with equal contribution.

References

1) Agner, K. Detoxicating effect of verdoperoxidase on toxins. *Nature.* **1947***, 159*, 271-272.

2) Harrison, J. E.; Schultz J. Studies on the chlorinating activity of myeloperoxidase. *J. Biol. Chem.* **1976**, *251*, 1371- 1374.

3) Klebanoff, S. J. Myeloperoxidase: Friend and foe. *J. Leukocyte Biol.* **2005,** *77*, 598-562.

4) Schultz, J.; Kaminker, K. Myeloperoxidase of the leukocyte of normal human blood. I. Content and localization. *Arch. Biochem. Biophys.* **1962,** *96*,465- 467.

5) Salmon, S. E.; Cline, M. J.; Schultz, J.; Lehrer, R. I. Myeloperoxidase deficiency. Immunologic study of a genetic leukocyte defect. *N. Engl. J. Med.* **1970***, 282*, 250-253.

6) Fiedler, T. J.; Davey, C.; Fenna, R. X-ray crystal structure and characterization of halide-binding sites of human myeloperoxidase at 1.8 A resolution. *J. Biol. Chem.* **2000**, *275*, 11964- 11971.

7) Furtmüller, P.; Burner, U.; Obinger, C. Reaction of human myeloperoxidase compound I with chloride, bromide, iodide, and thiocyanate. *Biochemistry.* **1998**, *37*, 17923-17930.

8) Zederbauer, M.; Furtmüller, P. G.; Brogioni, S.; Jakopitsch, C.; Smulevich, G.; Obinger, C.. Heme to protein linkages in mammalian peroxidases: Impact on spectroscopic, redox and catalytic properties. *Nat. Prod. Rep*. **2007**, *24*, 571-584.

9) Jantschko, W.; Furtmüller, PG.; Zederbauer, M.; Neugschwandtner, K.; Lehner, I.; Jakopitsch, C.; Arnhold, J.; Obinger, C. Exploitation of the unusual thermodynamic properties of human myeloperoxidase in inhibitor design. *Biochem. Pharmacol.* **2005**, *69*,1149- 1157.

10) Nicholls, S.; Hazen, S. Myeloperoxidase and cardiovascular disease. *Arterioscler. Thromb. Vasc. Biol.* **2005***, 25*, 1102-1111.

11) Hazen, S. Myeloperoxidase and plaque vulnerability," *Arterioscler. Thromb. Vasc. Biol.* **2004***, 24*, 1143-1146.

12) Van Antwerpen, P.; Dufrasne, F.; Lequeux, M.; Zouaoui-Boudjeltia, K.; Lessgyer, I.; Babar, S.; Moreau, P.; Moguilevsky, N.; Vanhaeverbeek, M.; Ducobu, J.; Neve, J. Inhibition of the myeloperoxidase chlorinating activity by non-steroidal anti-inflammatory drugs: Flufenamic acid and its 5-chloro-derivative directly interact with a recombinant human myeloperoxidase to inhibit the synthesis of hypochlorous acid. *Eur. J. Pharmacol.* **2007***, 570*,235- 243.

13) Soubhye, J.; Prévost, M.; Van Antwerpen, P.; Boudjeltia, K.; Rousseau, A.; Furtmüller, PG.; Obinger, C.; Vanhaeverbeek, M.; Ducobu, J.; Neve, J.; Gelbcke, M.; Dufrasne, F. Structure-based design, synthesis, and pharmacological evaluation of 3-(aminoalkyl)-5-fluoroindoles as myeloperoxidase inhibitors. *J. Med. Chem.* **2010***, 53*, 8747- 8759.

14) Forbes, L.; Sjögren, T.; Auchère, F.; Jenkins, D.; Thong, B.; Laughton, D.; Hemsley, P.; Pairaudeau, G.; Turner, R.; Eriksson, H.; Unitt, J.; Kettle, A. Potent reversible inhibition of myeloperoxidase by aromatic hydroxamates. *J. Biol. Chem.* **2013,** *288*, 36636-36647.

15) Roth, A.; Ott, S.; Farber, K.; Palazzo, T.; Conrad, W.; Haddadin, M.; Tantillo, D.; Cross, C.; Eiserich J.; Kurth, M. Inhibition of myeloperoxidase: evaluation of 2H-indazoles and 1H-indazolones. *Bioorg. Med. Chem.* **2014**, *22*, 6422-6429.

16) Blair-Johnson, M.; Fiedler, T.; Fenna, R. Human myeloperoxidase: structure of a cyanide complex and its interaction with bromide and thiocyanate substrates at 1.9 A resolution. *Biochemistry.* **2001**, *40*, 13990-13997.

17) Tidén, A. K.; Sjögren, T.; Svensson, M.; Bernlind, A.; Senthilmohan, R.; Auchère, F.; Norman, H., Markgren, P. O.; Gustavsson, S.; Schmidt, S.; Lundquist, S.; Forbes, L. V.; Magon, N. J.; Paton, L. N.; Jameson, G. N.; Eriksson, H.; Kettle, A. 2-Thioxanthines are mechanism-based inactivators of myeloperoxidase that block oxidative stress during inflammation. *J. Biol. Chem.* **2011**, *286*, 37578- 37589.

18) Davey, C.; Fenna, R. 2.3 A resolution X-ray crystal structure of the bisubstrate analogue inhibitor salicylhydroxamic acid bound to human myeloperoxidase: a model for a prereaction complex with hydrogen peroxide. *Biochemistry.* **1996**, *35*, 10967-10973.

19) Van Antwerpen, P.; Prévost, M.; Zouaoui-Boudjeltia, K.; Babar, S.; Legssyer, I.; Moreau, P.; Moguilevsky, N.; Vanhaeverbeek, M.; Ducobu, J.; Neve, J.; Dufrasne, F. Conception of myeloperoxidase inhibitors derived from flufenamic acid by computational docking and structure modification. *Bioorg. Med. Chem.* **2008**, *16*, 1702- 1720.

20) Aldib, I.; Soubhye, J.; Zouaoui Boudjeltia, K.; Vanhaeverbeek, M.; Rousseau, A.; Furtmüller, PG.; Obinger, C.; Dufrasne, F.; Nève, J.; Van Antwerpen, P.; Prévost, M. Evaluation of new scaffolds of myeloperoxidase inhibitors by rational design

combined with high-throughput virtual screening. *J. Med. Chem.* **2012***, 55*, 7208-7218.

21) Soubhye, J.; Aldib, I.; Delporte, C.; Prévost, M.; Dufrasne, F.; Van Antwerpen, P. Myeloperoxidase as a target for treatment of inflammatory syndromes: mechanisms and structure activity relationships of inhibitors. *Curr. Med. Chem*. **2016**, *23*, 3975-4008.

22) Malvezzi, A.; Queiroz, R. F.; De Rezende, L.; Augusto, O.; do Amaral, A. T. MPO inhibitors selected by virtual screening. *Mol. Inform.* **2011***, 30*, 605- 613.

23) Wolber, G.; Langer, T. LigandScout: 3-D pharmacophores derived from protein-bound ligands and their use as virtual screening filters, *J. Chem. Inf. Model*. **2005,** *45*, 160-169.

24) Soubhye, J.; Alard, IC.; van Antwerpen, P.; Dufrasne, F. Type 2 17-β hydroxysteroid dehydrogenase as a novel target for the treatment of osteoporosis. *Future Med. Chem*. **2015**, *7*, 1431-1456.

25) Vuorinen, A.; Engeli, R.; Meyer, A.; Bachmann, F.; Griesser, U.; Schuster, D.; Odermatt, A. Ligand-based pharmacophore modeling and virtual screening for the discovery of novel 17β-hydroxysteroid dehydrogenase2 inhibitors. *J.Med.Chem.* **2014**, *57*, 5995-6007.

26) Venugopala, K.; Govender, R.; Khedr, M.; Venugopala, R.; Aldhubiab, B.; Harsha, S.; Odhav, B. Design, synthesis, and computational studies on dihydropyrimidine scaffolds as potential lipoxygenase inhibitors and cancer chemopreventive agents. *Drug. Des. Devel. Ther.* **2015***, 9*, 911-921.

27) Irwin, J.; Shoichet, BK. ZINC--a free database of commercially available compounds for virtual screening. *J. Chem. Inf. Model.* **2005***, 45*, 177-182.

28) Soubhye, J.; Aldib, I.; Prévost, M.; Elfving, B.; Gelbcke, M.; Podrecca, M.; Conotte, R.; Colet, J.; Furtmüller, PG..; Delporte, C.; Rousseau, A.; Vanhaeverbeek, M.; Nève, J.; Obinger, C.; Zouaoui-Boudjeltia, K.; Van Antwerpen, P.; Dufrasne, F. Hybrid molecules inhibiting myeloperoxidase activity and serotonin reuptake: a possible new approach of major depressive disorders with inflammatory syndrome. *J. Pharm. Pharmacol,* **2014**, *66*, 1122-1132.

29) Soubhye, J.; Aldib, I.; Elfving, B.; Gelbcke, M.; Furtmüller, PG.; Podrecca, M.; Conotte, R.; Colet, J.; Rousseau, A.; Reye, F.; Sarakbi, A. Vanhaeverbeek, M.; Kauffmann , J.M.; Obinger, C.; Nève, J.; Prévost, M.; Zouaoui-Boudjeltia, K.; Van Antwerpen, P.; Dufrasne, F. Design, synthesis, and structure-activity relationship studies of novel 3-alkylindole derivatives as selective and highly potent myeloperoxidase inhibitors. *J. Med. Chem.* **2013***, 56*, 3943-3958.

30) Zeraik, M.; Ximenes, V.; Regasini, L.; Dutra, L.; Silva, D.; Fonseca, L.; Coelho, D.; Machado, S.; Bolzani, V. 4'-Aminochalcones as novel inhibitors of the chlorinating activity of myeloperoxidase. *Curr. Med. Chem.* **2012**, *19*, 5405-5413.

31) Boufadi, Y.; Soubhye, J.; Riazi, A.; Rousseau, A.; Vanhaeverbeek, M.; Nève, J.; Boudjeltia, K.; Van Antwerpen, P. Characterization and antioxidant properties of six Algerian propolis extracts: ethyl acetate extracts inhibit myeloperoxidase activity. *Int. J. Mol. Sci.* **2014***, 15*, 2327-2345.

32) Kleszczyński, K.; Hardkop, L.; Fischer, T. Differential effects of melatonin as a broad range UV-damage preventive dermato-endocrine regulator. *Dermatoendocrinol,* **2011**, *3*, 31-27.

33) Van Antwerpen, P.; Dufrasne, F.; Lequeux, M.; Boudjeltia, K.; Lessgyer, I.; Babar, S.; Moreau, P.; Moguilevsky, N.; Vanhaeverbeek, M.; Ducobu, J.; Nève, J. Inhibition of the myeloperoxidase chlorinating activity by non-steroidal anti-inflammatory drugs: flufenamic acid and its 5-chloro-derivative directly interact with a recombinant human myeloperoxidase to inhibit the synthesis of hypochlorous acid. *Eur. J. Pharmacol.* 2007*, 570*, 235-243.

34) Ruggeri, RB.; Buckbinder, L.; Bagley, SW.; Carpino, PA.; Conn, EL.; Dowling, MS.; Fernando, DP.; Jiao, W.; Kung, DW.; Orr, ST.; Qi, Y.; Rocke, BN.; Smith, A.; Warmus, JS.; Zhang, Y.; Bowles, D.; Widlicka, DW.; Eng, H.; Ryder, T.; Sharma, R.; Wolford, A.; Okerberg, C.; Walters, K.; Maurer, TS.; Zhang, Y.; Bonin, PD.; Spath, SN.; Xing, G.; Hepworth, D.; Ahn, K.; Kalgutkar, AS. Discovery of 2-(6-(5-chloro-2-methoxyphenyl)-4-oxo-2-thioxo-3,4-dihydropyrimidin-1(2H)-yl)acetamide (PF-06282999): a highly selective mechanism-based myeloperoxidase inhibitor for the treatment of cardiovascular diseases. *J. Med. Chem*. **2015**, *58*, 8513-8528.

35) Egan, R.; Hagmann, W.; Gale, P. Naphtalenes as inhibitors of myeloperoxidase: direct and indirect mechanisms of inhibition. *Agents. Actions.* **1990***, 29*, 266-276.

36) Nève, J.; Parij, N.; Moguilevsky, N.Inhibition of the myeloperoxidase chlorinating activity by non-steroidal anti-inflammatory drugs investigated with a human recombinant enzyme. *Eur. J. Pharmacol.* **2001***, 417*, 37-43.

37) Kettle, A.; Winterbourn, C. Mechanism of inhibition of myeloperoxidase by anti-inflammatory drugs. *Biochem. Pharmacol.* **1991**. *41*, 1485-1492.

38) Sinha, B.; Mason, R. Biotransformation of hydrazine derivatives in the mechanism of toxicity. *J. Drug. Metab. Toxicol* [online] **2014**, *5*, 168.

39) Webb, T.; Lvovskiy, L.; Kim, S.; Ji, X.; Melman, N.; Linden J.; Jacobson, K. Quinazolines as adenosine receptor antagonists: SAR and selectivity for A2B receptors. *Bioorg. Med. Chem.* **2003***, 11*, 77-85.

40) Cheng, F.; Li, W; Zhou, Y.; Shen, J.; Wu, Z.; Liu, G.; Lee, P.; Tang, Y. admetSAR: a comprehensive source and free tool for assessment of chemical ADMET properties. *J. Chem. Inf. Model.* **2012**, *52*, 3099-3105.

41) Zámocký, M.; Hofbauer, S.; Schaffner, I.; Gasselhuber, B.; Nicolussi, A.; Soudi, M.; Pirker, K. F.; Furtmüller, P. G.; Obinger, C.. Independent evolution of four heme peroxidase superfamilies. *Arch. Biochem. Biophys*. **2015**, *574*, 108-119.

42) Sutherland, J.; Nandigam, R.; Erickson, J.; Vieth, M. Lessons in molecular recognition. 2. Assessing and improving cross-docking accuracy. *J. Chem. Inf. Model.* **2007***, 47*, 2293-22302.

43) Soubhye, J.; Meyer, F.; Furtmüller, PG.; Obinger, C.; Dufrasne, F.; van Antwerpen, P. Characterization of chemical features of potent myeloperoxidase inhibitors. *Future Med. Chem*. **2016**, *8*, 1163-1177.

44) Carr, A. C.; Myzak, M. C.; Stocker, R.; McCall, M. R.; Frei, B. Myeloperoxidase binds to low-density lipoprotein: potential implications for atherosclerosis *FEBS Lett.* **2000**, *487*, 176- 180.

45) Van Antwerpen, P.; Prévost, M.; Zouaoui-Boudjeltia, K.; Babar, S.; Legssyer, I.; Moreau, P.; Moguilevsky, N.; Vanhaeverbeek, M.; Ducobu, J.; Nève, J.; Dufrasne, F. Conception of myeloperoxidase inhibitors derived from flufenamic acid by computational docking and structure modification *Bioorg. Med. Chem*. **2008**, *16*, 1702- 1720.

46) Ross-Lee, L.; Eadie, M.; Hooper, W.; Bochner, F. Single-dose pharmacokinetics of metoclopramide. *Eur.J.Clin. Pharmacol.* **1981**, *20*, 465-471.

47) Shepherd, A.; McNay, J.; Ludden, M.; Lin, M.; Musgrave, G. Plasma concentration and acetylator phenotype determine response to oral hydralazine. *Hypertension*. **1981**, *3*, 580-585.

48) Soubhye, J.; Gelbcke, M.; Van Antwerpen, P.; Dufrasne, F.; Boufadi, MY.; Nève, J.; Furtmüller, PG.; Obinger, C.; Zouaoui Boudjeltia, K.; Meyer, F. From dynamic combinatorial chemistry to in vivo evaluation of reversible and irreversible myeloperoxidase inhibitors. *ACS. Med. Chem. Lett*. **2016**, *8*, 206-210.

49) Rarey, M.; Kramer, B.; Lengauer, T.; Klebe, G. A fast flexible docking method using an incremental construction algorithm. *J. Mol. Biol.* **1996**, *261*, 470-89.

50) Schneider, N.; Hindle, S.; Lange, G.; Klein, R.; Albrecht, J.; Briem, H.; Beyer, K.; Claußen, H.; Gastreich, M.; Lemmen, C.; Rarey, M. Substantial improvements in large-scale redocking and screening using the novel HYDE scoring function. *J. Comput. Aided. Mol. Des.* **2012**, *26*, 701-23.

51) Friesner, RA.; Murphy, RB.; Repasky, MP.; Frye, LL.; Greenwood, JR.; Halgren, TA.; Sanschagrin, PC.; Mainz DT. Extra precision glide: docking and scoring incorporating a model of hydrophobic enclosure for protein-ligand complexes. *J. Med. Chem.* **2006,** *49*, 6177-6196.

52) Greenwood, JR.; Calkins, D.; Sullivan, AP.; Shelley, JC. Towards the comprehensive, rapid, and accurate prediction of the favorable tautomeric states of drug-like molecules in aqueous solution. *J. Comput. Aided. Mol. Des.* **2010,** *24*, 591-604.

53) Furtmüller, PG.; Burner, U.; Obinger, C. Reaction of human myeloperoxidase Compound I with chloride, bromide, iodide, and thiocyanate. *Biochemistry.* **1998**, *37*, 17923- 17930.

54) Hewson, W. D.; Hager, L. P. Mechanism of the chlorination reaction catalyzed by horseradish peroxidase with chlorite *J. Biol. Chem.* **1979**, *254*, 3175- 3181.

55) Havel, R. J.; Eder, H. A.; Bragdon, J. H. Distribution and chemical composition of ultracentrifugally separated lipoproteins in human serum *J. Clin. Invest.* **1955**, *34*, 1345- 1353.

56) Van Antwerpen, P.; Boudjeltia-Zouaoui, K.; Babar, S.; Legssyer, I.; Moreau, P.; Moguilevsky, N.; Vanhaeverbeek, M.; Ducobu, J.; Nève, J. Thiol-containing molecules interact with the myeloperoxidase/H2O2/chloride system to inhibit LDL oxidation *Biochem. Biophys. Res. Commun.* **2005**, *337*, 82- 88.

57) Furtmüller, G.P.; Obinger, C.; Prévost, M.; Van Antwerpen, P.; Arnhold, J.; Flemmig, J. Flavonoids as promoters of the (pseudo-)halogenating activity of lactoperoxidase and myeloperoxidase. *Free. Radic. Biol. Med.* **2016**, *97*, 307-319.

58) Mosmann, T.; Rapid colorimetric assay for cellular growth and survival: application to proliferation and cytotoxicity assays. *J. Immunol .Methods.* **1983**; *65*,55–63.

59) Flemmig, J.; Lessig, J.; Reibetanz, U.; Dautel P.; Arnhold, J. Non-vital polymorphonuclear leukocytes express myeloperoxidase on their surface. *Cell. Physiol. Biochem.* **2008**, *21*, 287-296.

60) Kettle, A.; Gedye, C.; Winterbourn, C. Mechanism of inactivation of myeloperoxidase by 4-aminobenzoic acid hydrazide. *Biochem. J.* **1997**, *321*, 503-508.

61) Flemmig, J.; Remmler, J.; Rohring, F.; Arnhold, J. (-)-Epicatechin regenerates the chlorinating activity of myeloperoxidase in vitro and in neutrophil granulocytes. *J. Inorg. Biochem.* **2014**, *130*, 84-91.

62) Flemmig, J.; Remmler, J.; Zschaler, J.; Arnhold, J. Detection of the halogenating activity of heme peroxidases in leukocytes by aminophenyl fluorescein. *Free Radic. Res.* **2015**, *49*, 768-776.

63) Beers R. J.; Sizer, I. A spectrophotometric method for measuring the breakdown of hydrogen peroxide by catalase. *J. Biol. Chem*. **1952**, *195*, 133-140.

Tables

Table (1): Active and inactive compounds used to validate the filters. (+) means that the compound passed the filter and (-) means that the compounds failed.

Table (2): Lead compounds listed along with their IC_{50} (μM) obtained by taurine chloramine assay, their affinity of the best score docked position (Gscore, kcal/mol) and the model by which they were selected.

Table (3): Residual activity of 100 nM of MPO incubated with 5 μM of tested compound, after diluting the reaction mixture 100-folds. IC_{50} values for inhibition of oxidation of LDL mediated by the MPO/Cl^-/H_2O_2 system.

Table (4): Apparent bimolecular rate constants of reduction of MPO Compound I (k_3) and Compound II reduction (k_4) by **28**, **29**, **36**, **40**, and **43**.

Table (5): The synthesized compounds derived from **28** (compounds **56-62**) with their IC_{50} (nM) with the taurine chloramine assay and their affinity with the best score docked position (Gscore, kcal/mol).

Table (6): Predicted and experimental ADME/T profiles of the selected inhibitors.

Table (7): Selectivity of the best MPO inhibitors versus LPO.

Table 1:

Compounds	Structures	Lipinski's Filter	Pharmacophore Screening	Docking screening	OSIRIS ® Property Explorer
Active compounds					
Chalcone (8)[30]	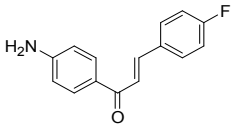	Passed	Models 1 and 2	Passed	Passed
Ferulic AC (9)[31]	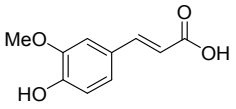	Passed	Model 4	Passed	Passed
Melatonin (10)[32]	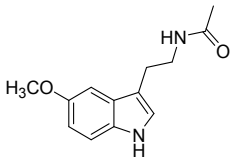	Passed	Model 4	Passed	Passed
Mefenamic AC (11)[33]	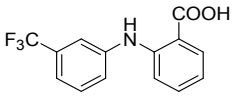	Passed	Model 3	Passed	Passed
12[34]	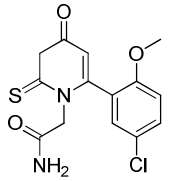	Passed	Model 4	Passed	Passed
Isoniazid (13) [22]	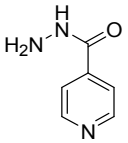	Passed	Model 1	Passed	Passed
14[35]	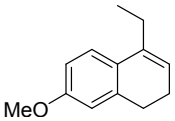	Passed	Model 3	Passed	Failed

15 [17]	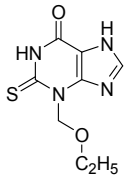	Passed	Failed	Passed	Passed
16 [20]	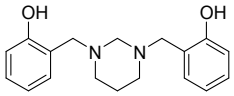	Passed	Model 1 and 3	Passed	Passed
17 [14]	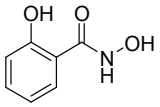	Passed	Model 2	Passed	Passed
Inactive compounds					
Tyrosine (18) [9]	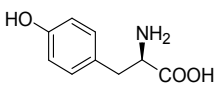	Passed	Failed	Failed	Failed
Fluoxetine (19) [28]	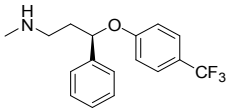	Passed	Model 1	Failed	Passed
20 [29]	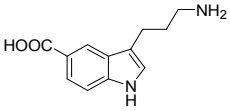	Failed	Model 2	Passed	Failed
21 [29]	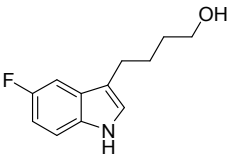	Failed	Failed	Failed	Passed
Diclofenac (22) [36]	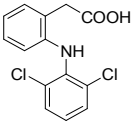	Passed	Failed	Failed	Passed
Piroxicam (23) [33]	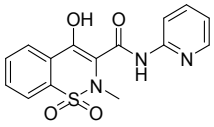	Passed	Failed	Failed	Passed

Sulindac (24) [33]	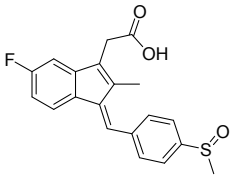	Passed	Failed	Failed	Passed
Naproxen (25) [36]	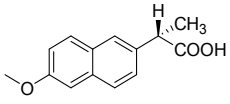	Passed	Model3	Failed	Passed
Chloroquine (26) [37]	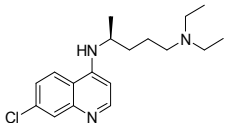	Passed	Failed	Passed	Passed
Antipyrine (27) [37]	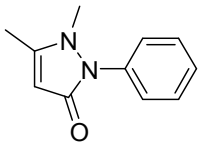	Passed	Failed	Failed	Passed

Table 2

Compounds	Structures	(IC_{50}, μM)*	ΔG (kcal/mol)	Model
28	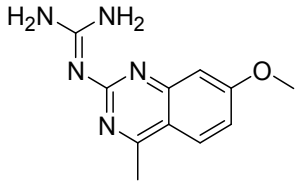	0.044 ± 0.005	-16.20	Model 1
Lomefloxacin **(29)**	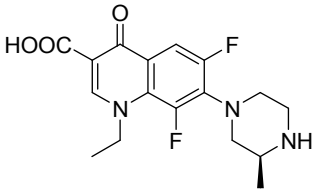	>5μM	-14.17	Model 1
Ciprofloxacine **(30)**	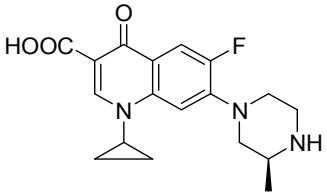	>5μM	-14.02	Model 1
Sulpiride **(31)**	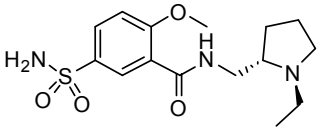	7.68 ± 1.32	-10.89	Model 1
Kumatakenin B **(32)**	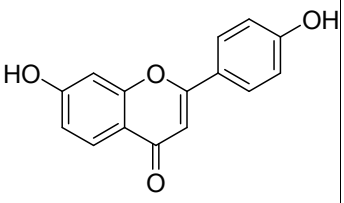	5.79 ± 0.58	-9.77	Model 1

Apegenin **(33)**	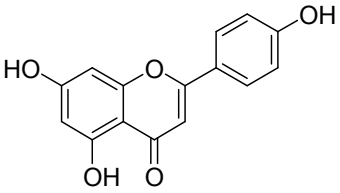	3.8 ± 0.44	-9.21	Model 1
Quercetin **(34)**	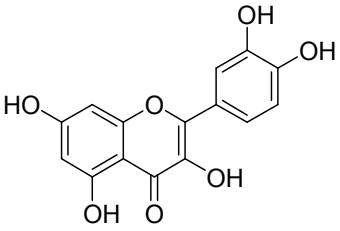	1.15 ± 0.09	-11.21	Model 1 (**PAINS**)
Kaempferol **(35)**	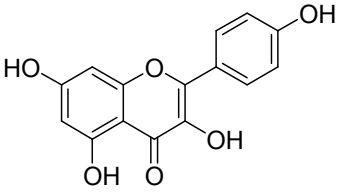	2.24 ± 0.12	-10.79	Model 1
Hydralazine **(36)**	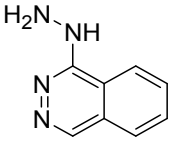	0.90 ± 0.12	-9.32	Model 1
Oxolinic acid **(37)**	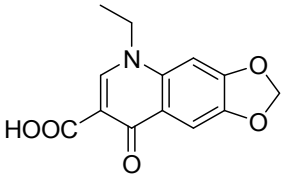	Not available	-9.10	Model 1
Triflupromazine **(38)**	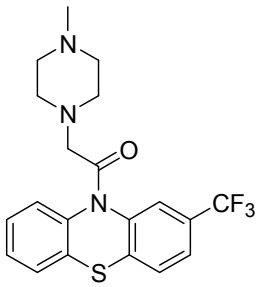	12.35% inhibition at 5μM	-11.70	Model 1 and 2

39	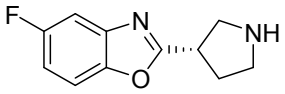	1.74 ± 0.08	-10.89	Model 1
Thioridazine **(40)**	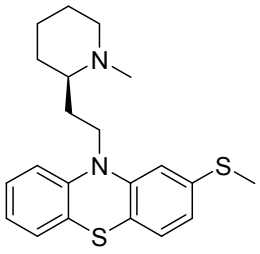	24.23% inhibition at 5μM	-11.22	Model 1 and 2
Primaquine **(41)**	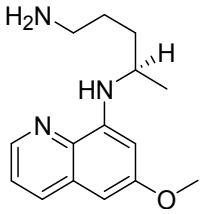	0.3 ± 0.01	-9.22	Model 1
42	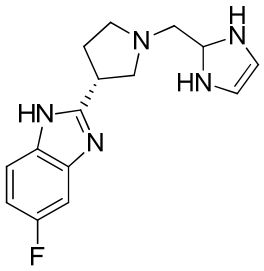	0.05 ± 0.009	-13.71	Model 1
43	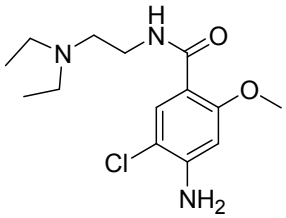	0.35 ± 0.03	-9.97	Model 1
Nifuroxazide **(44)**	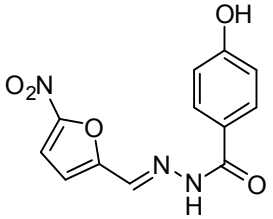	>5μM	-10.67	Model 2

45	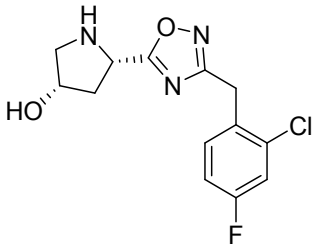	4.68 ± 1.07	-9.96	Model 2
46	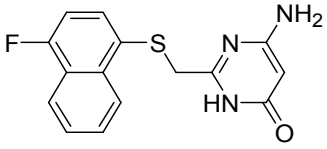	37.25% inhibition at 5μM	-8.63	Model 2
Celecoxib **(47)**	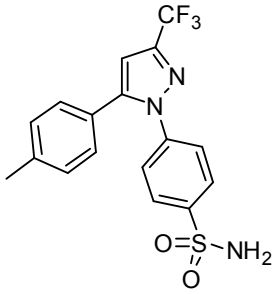	11.02% inhibition at 5μM	-8.22	Model 2
Mefenamic acid **(48)**	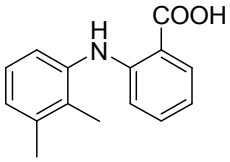	0.98 ± 0.02	-8.11	Model 2
Sulfadimethoxine **(49)**	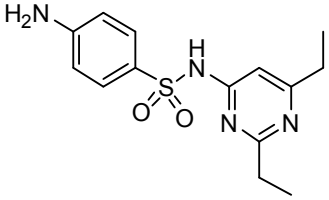	33.85% inhibition at 5 μM	-8.06	Model 2

50	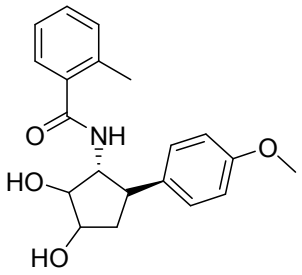	Not available	-9.68	Model 3
Isoxsuprine (**51**)	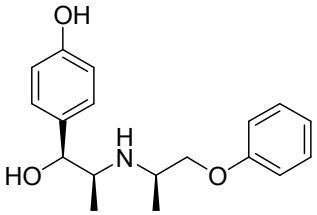	5.32% inhibition at 5μM	-8.88	Model 3
52	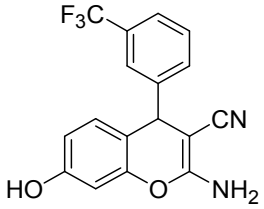	10.10 ± 2.8	-8.87	Model 3
53	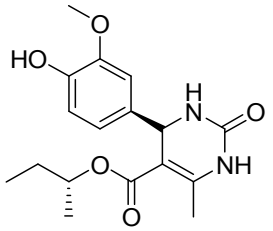	Not available	-8.36	Model 3
54	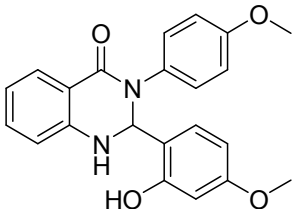	Not available	-8.02	Model 3 **(PAINS)**
55	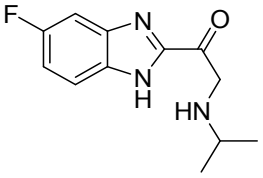	0.13 ± 0.02	-10.91	Model 4

*IC_{50} of the inhibition of MPO chlorination activity

Table 3

Compounds	Residual MPO activity without H_2O_2 (%)	Residual MPO activity with H_2O_2 (%)	Residual MPO activity with Cl^- + H_2O_2 (%)	LDL oxidation inhibition IC_{50} (µM)
28	84 ± 5	4 ± 3	5 ± 4	0.09 ± 0.03
34	72 ± 9	78 ± 8	79 ± 8	3.10 ± 0.21
35	78 ± 12	81 ± 6	84 ± 14	N.D
36	76 ± 8	9 ± 2	6 ± 13	2.36 ± 1.10
41	86 ± 4	91 ± 5	86 ± 8	N.D
42	83 ± 9	84 ± 8	84 ± 16	0.12 ± 0.06
43	91 ± 21	86 ± 7	83 ± 8	> 5
48	87 ± 12	82 ± 12	87 ± 15	2.21 ± 0.31
55	79 ± 24	87 ± 18	81 ± 14	N.D

Table 4

Compounds	k_3 ($M^{-1}s^{-1}$)	k_4 ($M^{-1}s^{-1}$)	IC_{50} (μM)
28	1.9×10^6	-	0.044 ± 0.005
29	3.1×10^4	1.2×10^3	Inactive*
36	7.1×10^6	-	0.90 ± 0.1
40	5.2×10^6	1.7×10^4	>5μM
43	2.6×10^6	180	1.0 ± 0.2

* Did not show any activity at 5 μM

Table 5

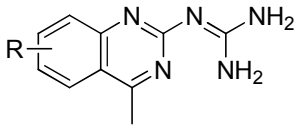

Compounds	R	IC_{50} (nM)	ΔG (kcal/mol)	Stacking pose
28	7-OMe	44 ± 0.5	-16.2	Stacking
56	H	900 ± 110	-12.85	Shift stacking
57	6-F	145 ± 30	-13.2	Stacking
58	6-Cl	630 ± 33	-10.5	No stacking
59	6-Br	756 ± 62	-10.5	No stacking
60	7-F	40 ± 9	-14.65	Stacking
61	7-Cl	96 ± 8	-12.65	Stacking
62	7-Br	106 ± 21	-12.15	Stacking

Table 6

Compound	Absorption			Metabolism	Toxicity			
	Blood-Brain Barrier	Human Intestinal Absorption	Caco-2 Permeability		Rat Acute Toxicity (LD50, mol/kg)	Carcinogenicity	*In Vitro* Growth Inhibition in NHDF& IC_{50} (μM)	Apoptosis of neutrophil at concentration of: (μM)
28	Yes*	Yes *	Yes *	CYP450 1A2 Inhibitor*	2.5210 **	No*	17#	> 50#
33	Yes *	Yes *	Yes *	CYP450 1A2 Inhibitor*, CYP450 3A4 Inhibitor*	2.6983**	No*	-	-
34	No**	Yes #	Yes *	CYP450 1A2 Inhibitor*, CYP450 3A4 Inhibitor**	3.0200*	No*	> 50#	-
35	Yes*	Yes*	Yes *	CYP450 1A2 Inhibitor*, CYP450 3A4	3.0825**	No*	-	-

				Inhibitor**				
36	Yes*	Yes#	Yes *	CYP450 1A2 substrate*, CYP450 3A4 inhibitor*	3.2187#	No#	> 50#	-
39	Yes*	Yes*	Yes **	CYP450 1A2 Inhibitor*	2.6350*	No*	> 50#	-
41	Yes*	Yes #	Yes **	CYP450 2D6 Substrate#, CYP450 3A4 Substrate#	2.4260**	No#	> 50#	-
42	Yes*	Yes*	Yes **	CYP450 1A2 Inhibitor**	2.7576**	No*	> 50#	> 50#
43	Yes #	Yes #	Yes #	CYP450 2C9 Substrate#, CYP450 2D6 Substrate#	2.602#	No#	> 50#	-
48	Yes*	Yes #	Yes #	CYP450 2C9 Substrate#	2.513#	No#	-	-

55	Yes*	Yes*	Yes **	CYP450 3A4 Substrate**, CYP450 1A2 Inhibitor**	2.6396**	No*	> 50#	-
60	Yes*	Yes*	Yes **	CYP450 1A2 Inhibitor*	2.8681**	No*	-	-

*Probability >0.8; **Probability <0.8; #Experimental value; NHDF: normal human dermal fibroblast, the IC_{50} values were obtained by MTT test.

Table 7

Compound	LPO IC_{50} (μM)	LPO (IC_{50})/MPO (IC_{50})
28	3.2 ± 0.2	73
33	17.8± 6.3	5.6
34	6.1± 2.3	5
35	ND	ND
36	1.2± 0.2	1.3
39	ND	ND
41	0.8± 0.1	3
42	>5	ND
43	>5	ND
48	ND	ND
55	>5	ND
60	3.9± 1.4	30

Figures

Figure (1): Scheme of chlorination and peroxidase cycles of myeloperoxidase (MPO). Reaction (1): native ferric MPO is oxidized by hydrogen peroxide to Compound I. In reaction (2), Compound I is directly reduced back to the native state by chloride or other (pseudo)halides, thereby releasing hypo(pseudo)halous acids. Reactions (1) and (2) constitute the halogenation cycle. In reaction (3), Compound I is reduced to Compound II via a one-electron process. In reaction (4), Compound II is reduced to the native form of MPO by a second electron donor. Reactions (1), (3), and (4) constitute the peroxidase cycle[13]. Compound III can only be formed from ferric or ferrous MPO with activated oxygen (reaction 6) or dioxygen (reaction 7) respectively. Reaction (5): Reduction of ferric to ferrous MPO by potential electron donors.

Figure (2): Structures of the most active MPO inhibitors with their IC_{50} values obtained by taurine chloramine test.

Figure (3): Schematic representation of the filter used to select the hits starting from 727,842 compounds of the Zinc ®database.

Figure (4): Pharmacophore models 1, 2, 3 and 4 for MPO inhibition. On the right side, the ensembles of compounds are represented as 2D structures. On the left side, the ensembles of compounds are aligned with the chemical features of the respective models. The pharmacophore features are color-coded: HBA, red; HBD, green; H, yellow; AR, blue. In the middle, the pharmacophore features with XVOLs.

Figure (5): Positions of some active compounds in MPO structure: (A) X-ray structure of human MPO in complex with compound **1** in green and docked pose of **1** in pink; **(B)** Docked

pose of compound **4**; **(C)** Docked pose of compound **6**; **(D)** Docked pose of compound **7** (3D structures of the compounds stacking on the heme of the active site).

Figure (6): View of the docked positions of **28** (A), **36**(B)**, 42** (C) and **55** (D). Red dotted lines depict strong interactions like salt bridges; the violet dotted lines depict week interactions like hydrogen bonds and π–π interaction.

Figure (7): (A) Probing the reversibility of MPO inhibition by **28** and **43**. Monitoring the absorbance at 470 nm during 400 seconds after adding 2 μM H_2O_2 and 30 μM guaiacol to the 200-fold diluted reaction mixtures which consist of MPO (50 nM) in 10 mM phosphate buffer (pH 7.4) and 5 μM of the inhibitor with 2 μM H_2O_2 (◆) **28**, (▲) **43** or without H_2O_2 (■) **28** (X) **43**. (B) The chlorinating activity of MPO during 600 s after the inhibition by **43** with or without the presence of tyrosine. (◆) **43** with tyrosine, (▲) **43** without tyrosine and (■) DMSO.

Figure (8): Reaction of MPO Compound I with **28** (pH 7.0 and 25 °C). (A) Initial spectral changes upon reaction of 2 μM MPO Compound I with 10 μM of **28**. The first spectrum was taken 5 ms after mixing, with subsequent spectra at 10, 15, 20, 26, 32, 38, 45, 58, 74, and 129 ms. Inset shows a typical time trace for the MPO Compound I reduction over the first 200 ms followed at 456 nm. (B) Continuation of (A). The first spectrum in (B) is identical to the last spectrum in (A). The first spectrum was taken at 129 ms and subsequent spectra were taken at 561 ms, 1.28 s, 2.1, 3.1, 4.1, 5.2, and 10 s. Inset shows the time traces at 429 nm and 456 nm. The red spectrum is Compound II, the blue spectrum is the last spectrum after 10 s that have a Soret maximum at 432 nm and a sharp band at 626 nm. Arrows indicate spectral changes. (C) Pseudo-first-order rate constants for MPO Compound I reduction plotted against **28** concentration. (D) Pseudo-first-order rate constants for MPO Compound II decay plotted against **28** concentration.

Figure (9): Reaction of MPO Compound I and II with **43** (pH 7.0 and 25 °C). (A) Spectral changes upon reaction of 2 μM of MPO Compound I with 20 μM of **43**. The first spectrum was taken 5 ms after mixing, with subsequent spectra at 10, 15, 20, 26, 32, 38, 58, and 100 ms. Inset shows a typical time trace for the MPO Compound I reduction over the first 200 ms followed at 456 nm. Red spectrum shows Compound II. (B) Spectral changes upon reaction of 2 μM of MPO Compound I with 500 μM of **43**. First spectrum was taken 0.04 s after mixing; subsequent spectra were taken at 8.5, 10.2, 11.3, 12.6, 14, 15.3, 16.1, 18.2, 20.8, 30.4, 40.5, 61.2, and 100 s. First spectrum (red) indicates Compound II last spectrum (green) shows the ferric MPO. Inset shows a typical time trace for the MPO Compound II reduction followed at 456 nm. Arrows indicate spectral changes. (C) Pseudo-first-order rate constants for MPO Compound I reduction plotted against concentration of **43**. (D) Pseudo-first-order rate constants for MPO Compound II reduction plotted against concentration of **43**.

Figure (10): Determination of the partition ratio for mechanism-based inactivation of MPO by **28, 36** and **43**. The fractional MPO activity of each inhibited reaction was plotted as a function of the ratio of inhibitor to MPO ([inhibitor]/[MPO]). Data are averages, and error bars represent the SD from two separate experiments. (◆)**28**, (■) and (▲) **43**.

Figure (11): View of the docked positions of **56** (A) and **60** (B). **56** shows shifted stacking while **60** features a stacking pose on the pyrrole D of the heme.

Figure (12): Proposal scheme of the oxidation of **36** (A) and **28** (B).

Figure 1

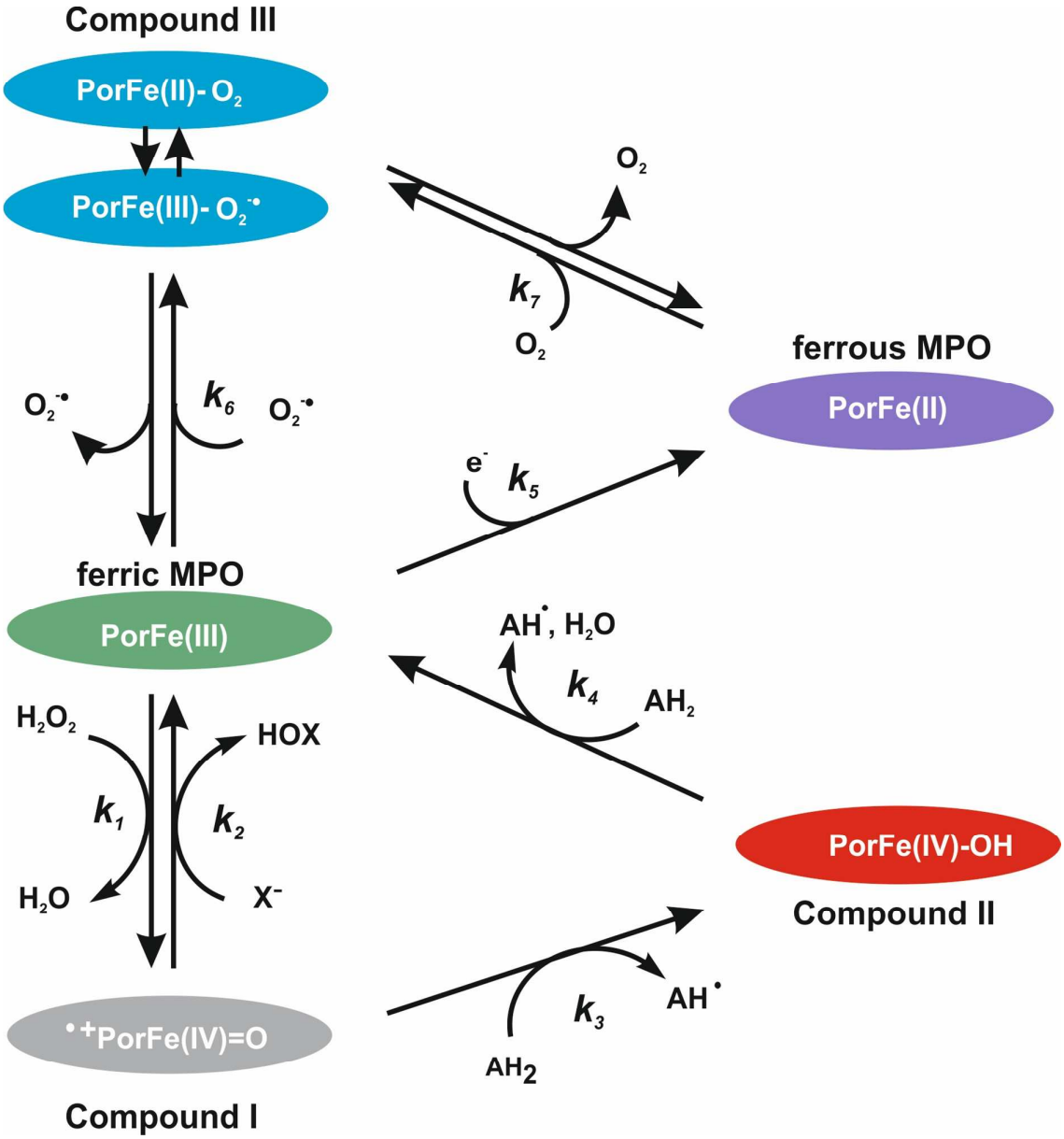
Compound III
PorFe(II)- O2
PorFe(III)- O2-•
O2-•
k6
O2-•
ferric MPO
PorFe(III)
H2O2
HOX
k1
k2
H2O
X-
•+PorFe(IV)=O
Compound I
O2
k7
O2
ferrous MPO
PorFe(II)
e-
k5
AH•, H2O
k4
AH2
PorFe(IV)-OH
Compound II
k3
AH•
AH2

Figure 2

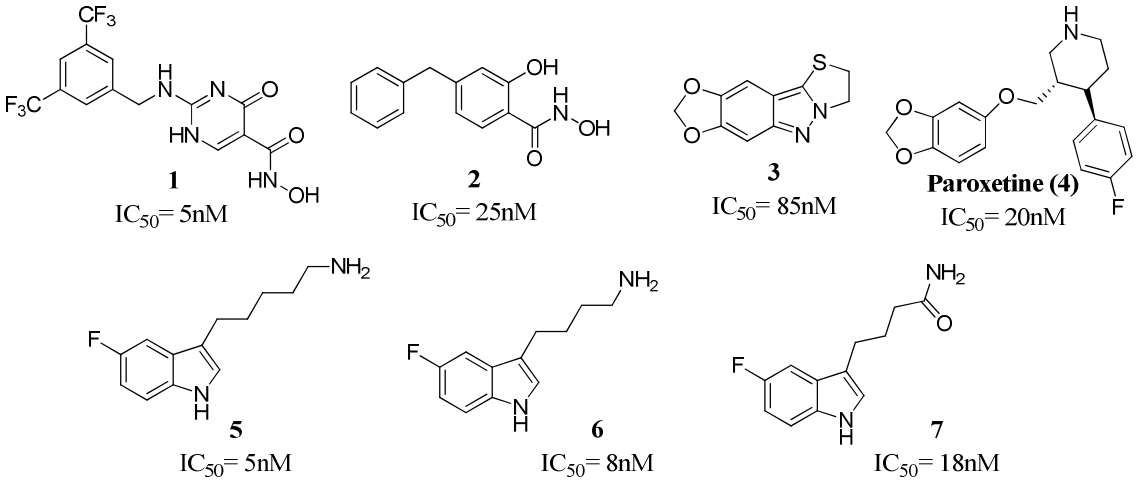
1
IC50= 5nM
2
IC50= 25nM
3
IC50= 85nM
Paroxetine (4)
IC50= 20nM
5
IC50= 5nM
6
IC50= 8nM
7
IC50= 18nM

Figure 3

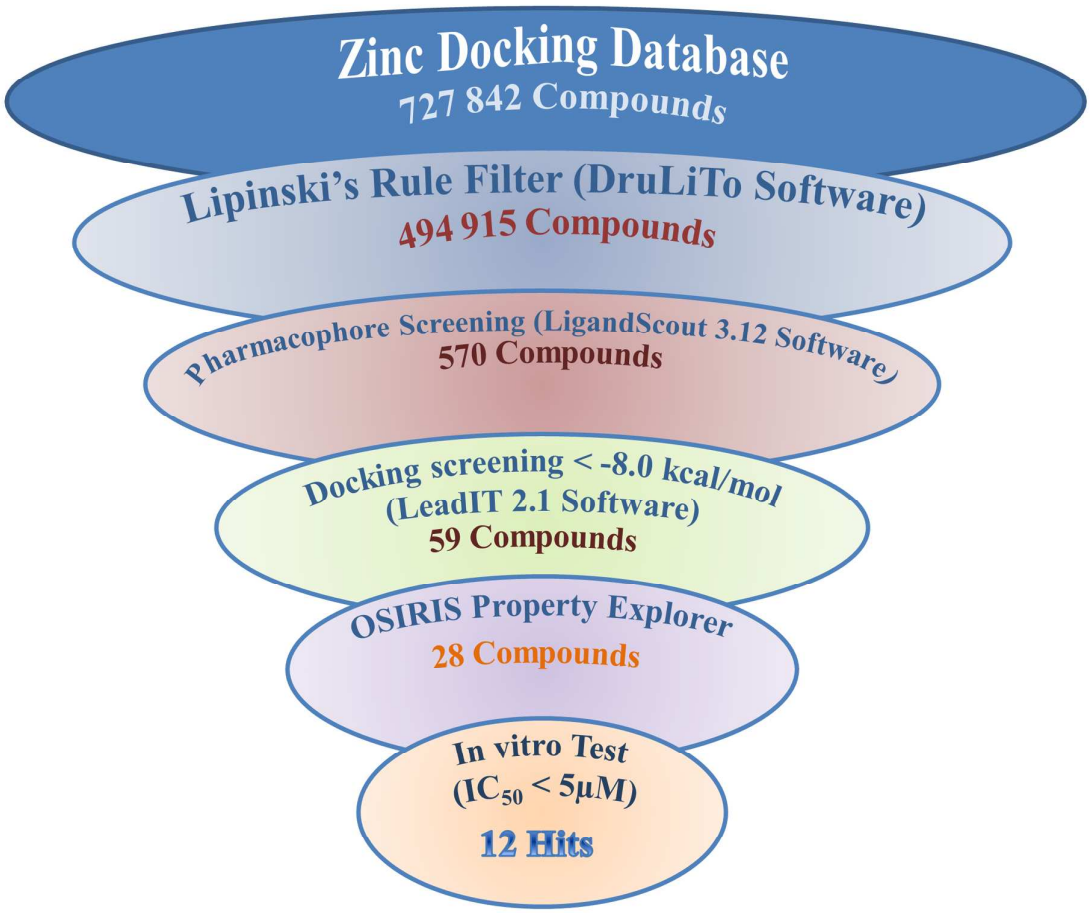
Zinc Docking Database
727 842 Compounds
Lipinski's Rule Filter (DruLiTo Software)
494 915 Compounds
Pharmacophore Screening (LigandScout 3.12 Software)
570 Compounds
Docking screening < -8.0 kcal/mol
(LeadIT 2.1 Software)
59 Compounds
OSIRIS Property Explorer
28 Compounds
In vitro Test
(IC50 < 5µM)
12 Hits

Figure 4

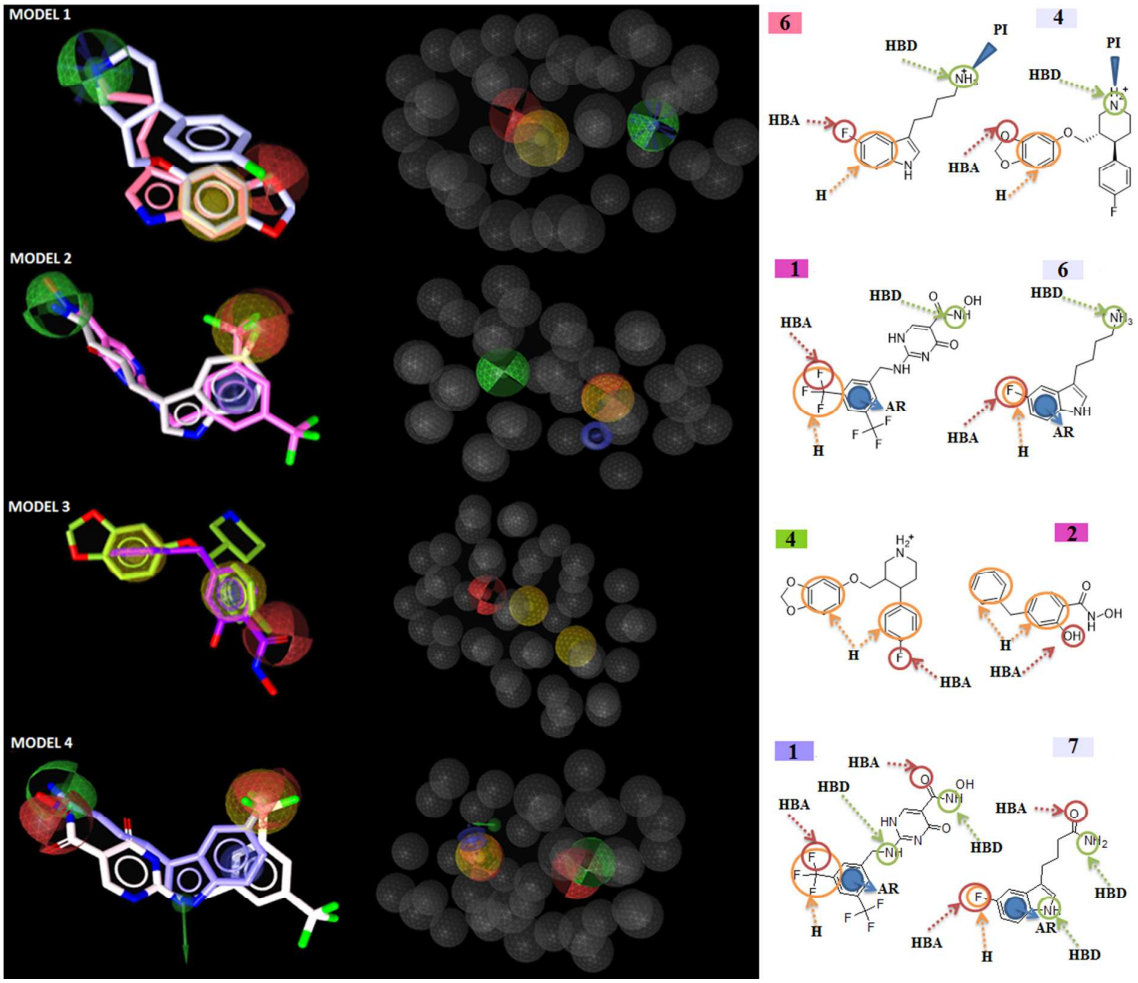

Figure 5

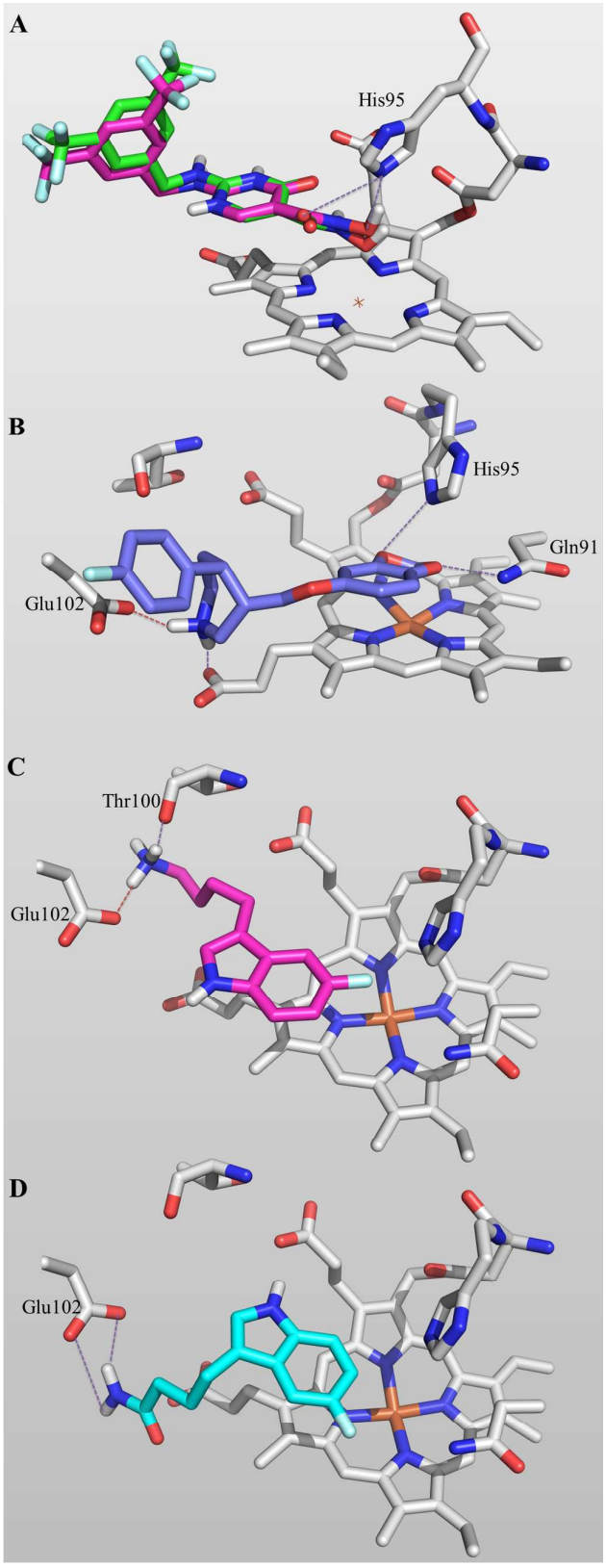

Figure 6

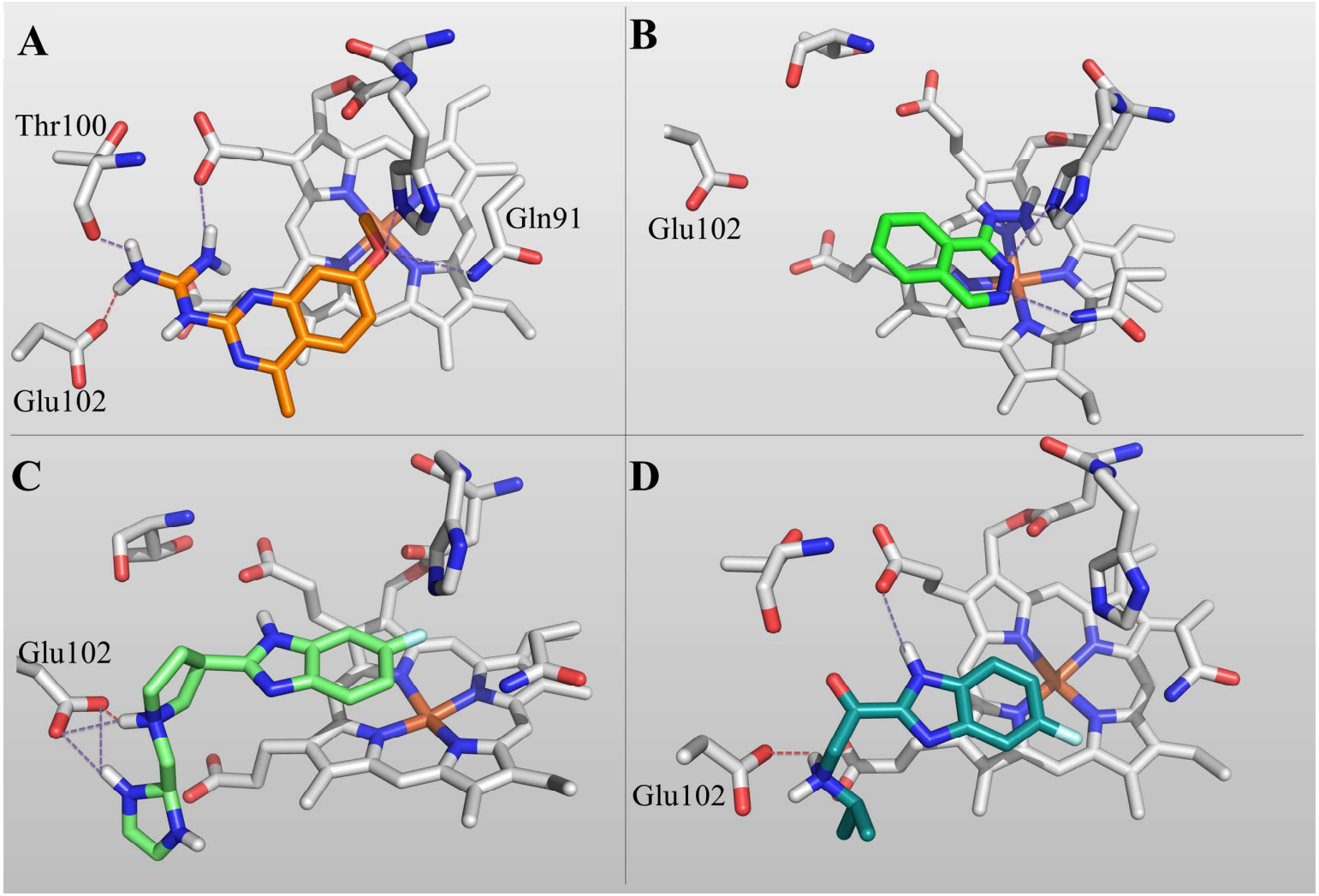

Figure 7

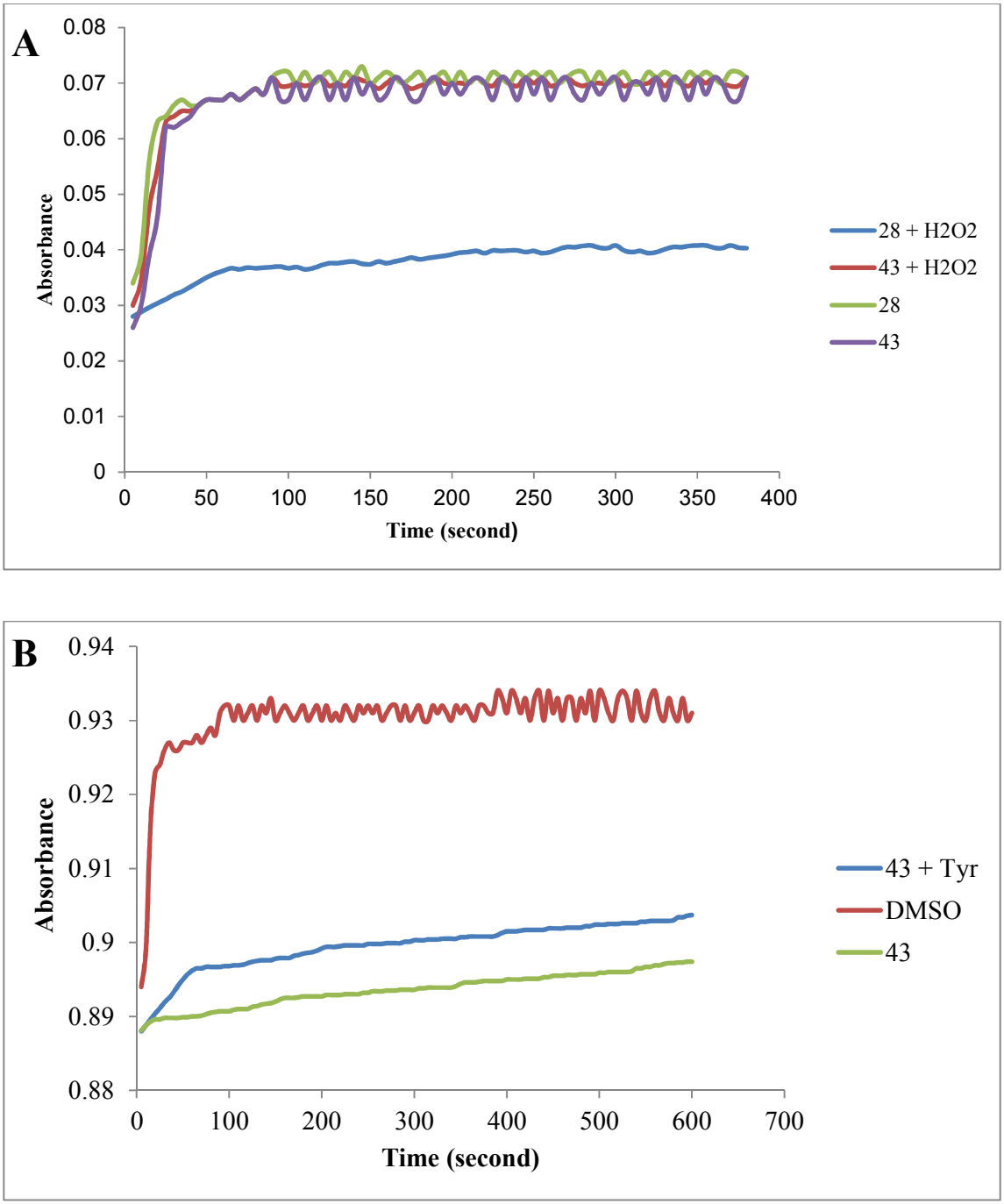
A
Absorbance
Time (second)
0.08
0.07
0.06
0.05
0.04
0.03
0.02
0.01
0
0
50
100
150
200
250
300
350
400
28 + H2O2
43 + H2O2
28
43
B
Absorbance
Time (second)
0.94
0.93
0.92
0.91
0.9
0.89
0.88
0
100
200
300
400
500
600
700
43 + Tyr
DMSO
43

Figure 8

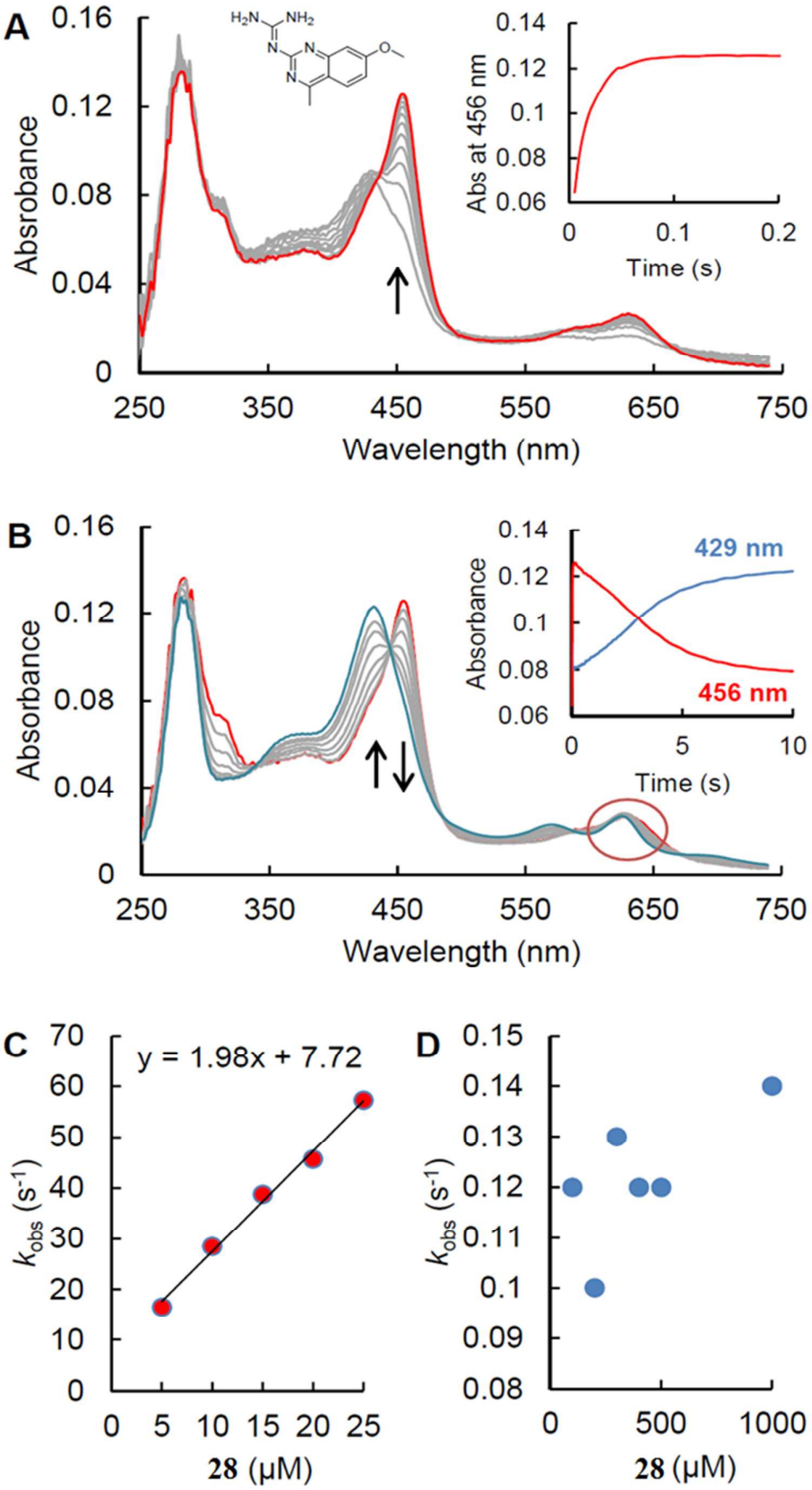
A
Absrobance
Wavelength (nm)
Abs at 456 nm
Time (s)
B
Absorbance
Wavelength (nm)
429 nm
456 nm
Time (s)
C
y = 1.98x + 7.72
k_{obs} (s^{-1})
28 (μM)
D
k_{obs} (s^{-1})
28 (μM)

Figure 9

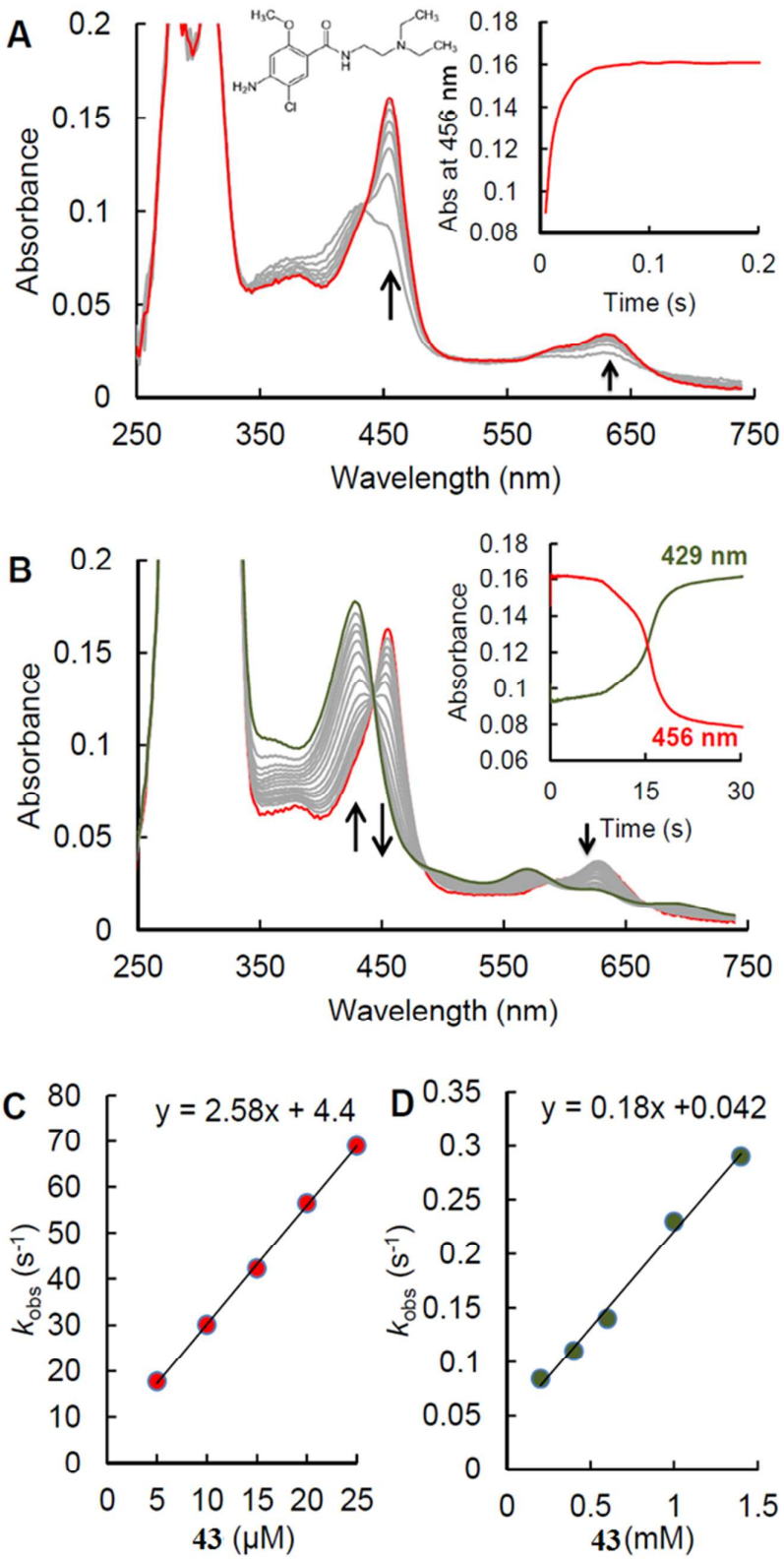
A
Absorbance
Wavelength (nm)
Abs at 456 nm
Time (s)
B
Absorbance
Wavelength (nm)
429 nm
456 nm
Time (s)
C
y = 2.58x + 4.4
k_{obs} (s^{-1})
43 (μM)
D
y = 0.18x +0.042
k_{obs} (s^{-1})
43 (mM)

Figure10

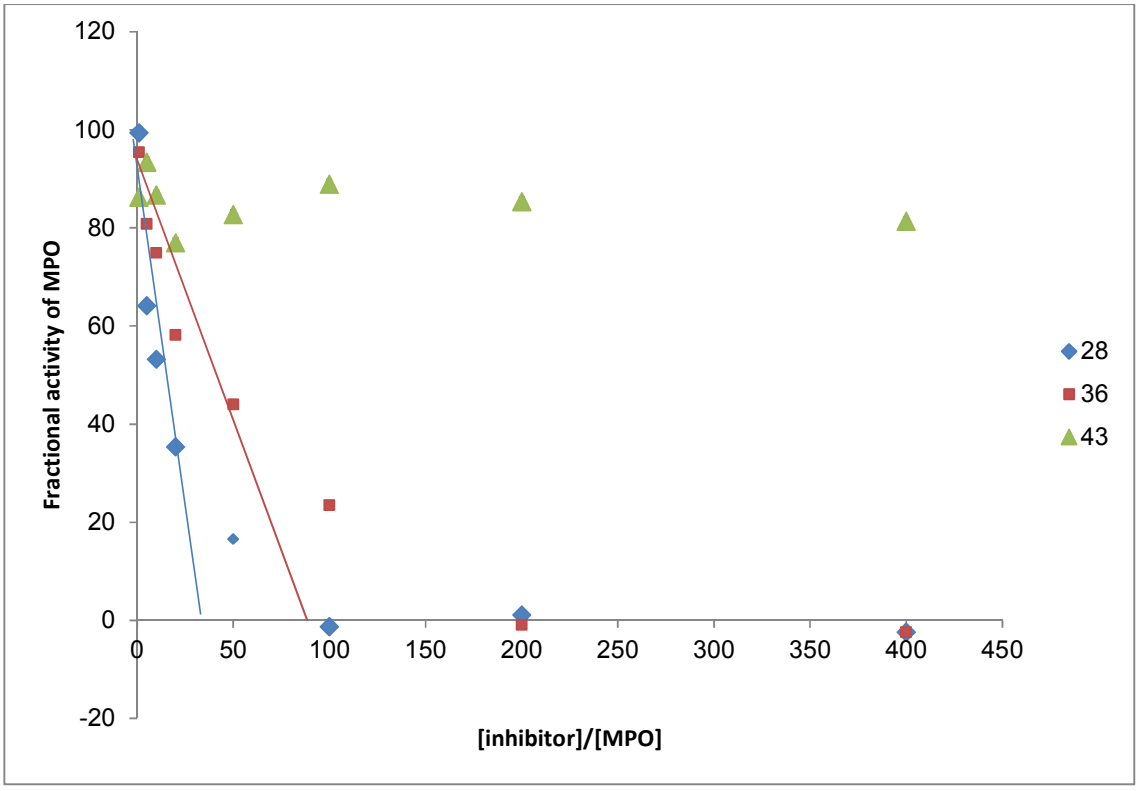
120
100
80
60
40
20
0
-20
0
50
100
150
200
250
300
350
400
450
Fractional activity of MPO
[inhibitor]/[MPO]
28
36
43

Figure 11

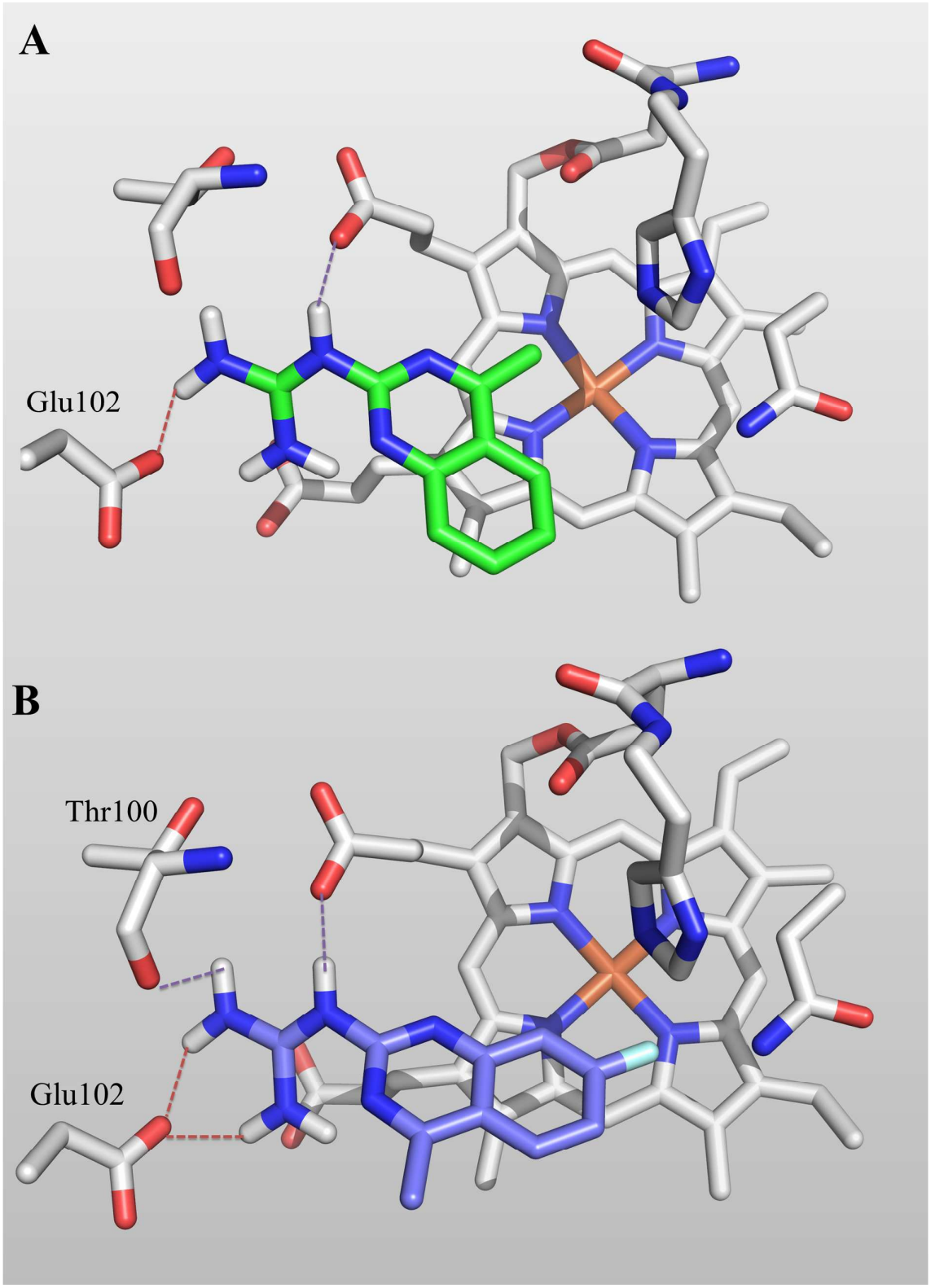

Figure 12

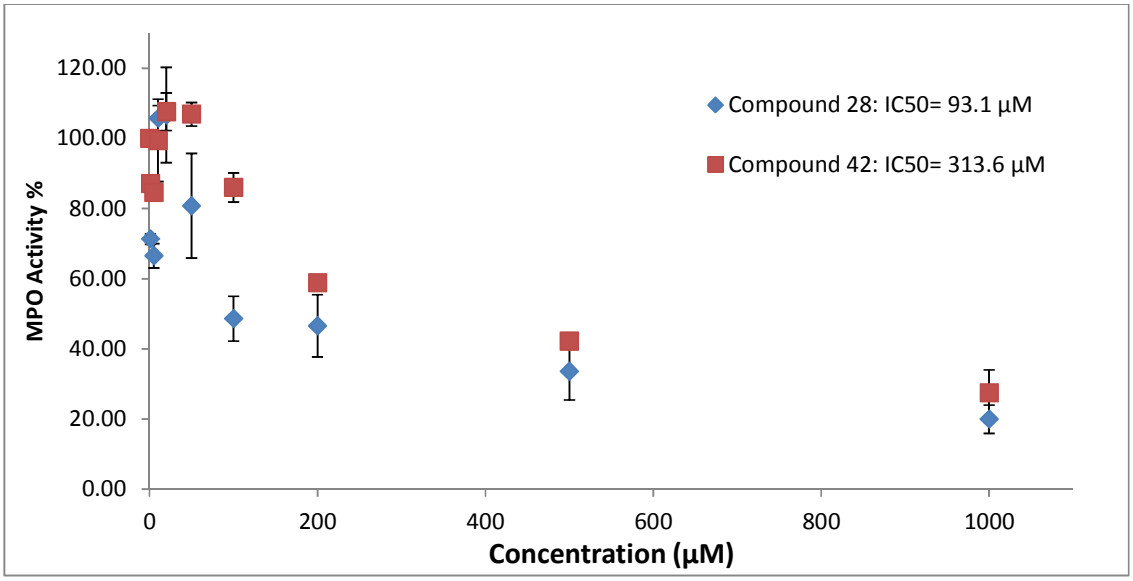
120.00
100.00
80.00
60.00
40.00
20.00
0.00
MPO Activity %
0
200
400
600
800
1000
Concentration (µM)
Compound 28: IC50= 93.1 µM
Compound 42: IC50= 313.6 µM

Figure 13

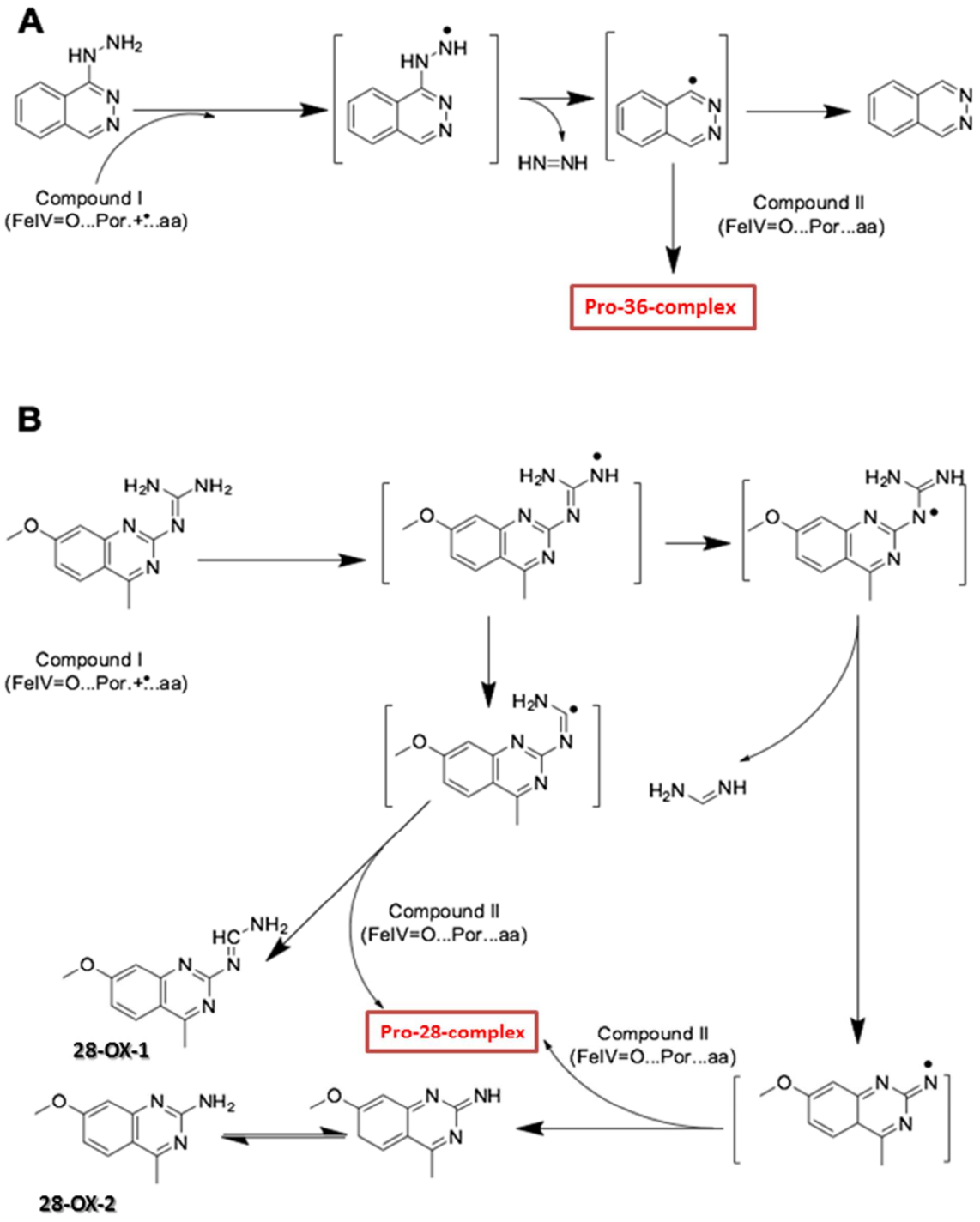
A
Compound I
(FeIV=O...Por.+•..aa)
HN=NH
Compound II
(FeIV=O...Por...aa)
Pro-36-complex
B
Compound I
(FeIV=O...Por.+•..aa)
Compound II
(FeIV=O...Por...aa)
Pro-28-complex
Compound II
(FeIV=O...Por...aa)
28-OX-1
28-OX-2

Scheme

Scheme (1): synthesis of *N*-(4-methyl-quinazolin-2-yl)-guanidine derivatives (**56-62**). (i) acetone, I_2, Δ, 3 days; (ii) HCl, Et_2O, CH_3CN 10 min, then dicyandiamide, KOH, Δ, 15h. R= H, F, Cl and Br at positions 6 and 7[37].

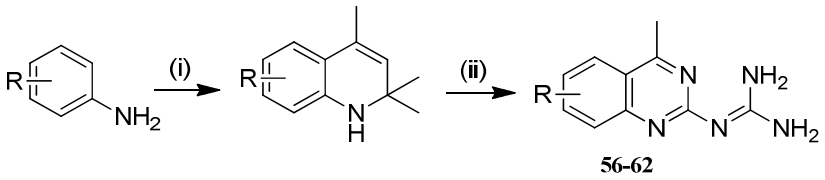

56-62

Graphical abstract